

## Fluid hydrogen at high density: Pressure dissociation

Didier Saumon

*Lunar and Planetary Laboratory, University of Arizona, Tucson, Arizona 85721*

Gilles Chabrier

*Laboratoire de Physique, Ecole Normale Supérieure Lyon, 69364 Lyon CEDEX 07, France*

(Received 8 February 1991)

We develop a model for the Helmholtz free energy of fluid hydrogen at high density and high temperature. This model aims at describing both pressure and temperature dissociation and ionization and bears directly on equations of state of partially ionized plasmas, as encountered in astrophysical situations and high-pressure experiments. This paper focuses on a mixture of hydrogen atoms and molecules and is devoted to the study of the phenomenon of pressure dissociation at finite temperatures. In the present model, the strong interactions are described with realistic potentials and are computed with a modified Weeks-Chandler-Andersen fluid perturbation theory that reproduces Monte Carlo simulations to better than 3%. Perturbations of the internal partition functions of H and H<sub>2</sub> arising in the nonideal fluid are treated self-consistently with a recently developed occupation probability formalism. Theoretical Hugoniot curves derived from our model are in excellent agreement with experimental data. Pressure dissociation occurs over a narrow density range above 0.5 g/cm<sup>3</sup> and is remarkably temperature insensitive. Molecules remain the dominant species even at high densities.

PACS number(s): 52.25.Jm, 64.30.+t, 05.70.Ce, 65.50.+m

### I. INTRODUCTION

The past decade has seen tremendous progress in our understanding of dense matter physics, on both the experimental and theoretical fronts. Dynamic compression experiments have revealed exciting new phenomena, such as pressure dissociation in (N<sub>2</sub>) [1,2], an increase of conductivity upon compression in an initially insulating material (O<sub>2</sub>) [3], and they have probed intermolecular potentials down to separations as small as 1.5 Å. In particular, experiments on hydrogen and deuterium have determined the H<sub>2</sub>-H<sub>2</sub> interaction potential at high densities [4].

Cryogenic samples of solid molecular hydrogen have been compressed to pressures of about  $2.5 \times 10^6$  atm, revealing a phase transition in the molecular solid and evidence for reduction of the band gap at the highest pressure reached [5–7]. This last phenomenon holds the promise of observing the much sought after metallic state of hydrogen in the near future.

On the other hand, the recent discovery of global oscillations in Jupiter [8] as well as the achievements of helio- and astero-seismology [9,10] give us new information on the interior structure of stars and giant planets, and consequently on the properties of matter under extreme thermodynamic conditions. They offer a unique chance to probe the accuracy of the theoretical models and stress the need for improved equations of state (EOS), particularly in the regime of partial ionization. Indeed, pressure ionization, as well as molecular dissociation, represents a thorny problem in modeling the properties of dense matter. Important advances in statistical physics over the last decade offer the opportunity for significant im-

provements in our comprehension of this poorly understood phenomenon.

Most of the extensive theoretical work on hydrogen has focused on the zero-temperature isotherm where it is now widely recognized that ionization may be accomplished by dissociation of the molecular phase into a monatomic metal or by closure of the conduction gap, which leads to a conducting molecular state [11,12]. We develop a free-energy model for fluid hydrogen which addresses the long-standing, difficult problems of pressure dissociation and ionization.

The simplified phase diagram shown on Fig. 1 helps to make a few essential points. In the low-density, low-temperature region, the hydrogen fluid is formed essentially of neutral particles and consists of atoms and molecules. Molecules dominate at low temperatures ( $\log_{10} T \lesssim 3.5$ ) [13] and they dissociate into atoms as the temperature is raised. At still higher temperatures, atoms ionize to form a low-density plasma of protons and electrons. The solid curves delimiting these three regions indicate a degree of dissociation (or ionization) of 50% and are based on the simple Saha equations for ionization equilibrium. At densities above  $\log_{10} \rho = -2$ , atoms and molecules interact strongly and form a nonideal fluid. Consequently, the Saha equations become inappropriate at such high densities and it is not possible to estimate the chemical equilibrium in this dense fluid with simple theories. The dotted line labeled  $r_s = 1$  indicates the density at which the nearest-neighbor separation between electrons is equal to the Bohr radius,  $a_0$ , a qualitative estimate of the location of pressure ionization. Above the line  $r_s = 1$ , hydrogen is fully ionized. The dash-dotted line on the left-hand side of the figure at  $\log_{10} \rho \approx -0.2$  is

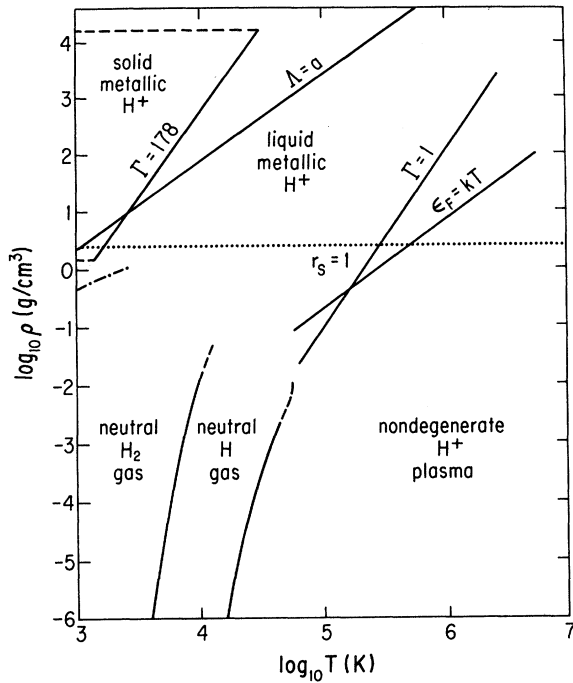


FIG. 1. Simplified  $(\rho, T)$  phase diagram for hydrogen. A few physical regimes are identified: above the line  $\Gamma=1$ , the plasma is strongly coupled, and electrons are degenerate above the line  $\epsilon_F=kT$ . Protons are classical below the line  $\Lambda=a$ . The dash-dotted line near  $\log_{10}\rho=0$  is the theoretical melting curve of  $H_2$  (Ref. [4]). Adapted from Fig. 2 of Ref. 67.

the theoretical melting curve for  $H_2$  [4]. Two important issues pertaining to the plasma are the degree of electron degeneracy  $\epsilon_F/kT$  ( $\epsilon_F$  is the Fermi energy of the electron gas) and the strength of the Coulomb coupling between the charged particles  $\Gamma=e^2/akT$  ( $a$  is the average interproton spacing). Protons remain classical over most of this diagram except above the line  $\Lambda=a$  ( $\Lambda$  denotes the de Broglie wavelength of the protons) where quantum effects become important. Above the line  $\Gamma=1$ , nonideal Coulomb effects play an important role. At  $\Gamma=178$ , the classical one-component plasma freezes into a solid lattice. However, since hydrogen is a very light element, quantum effects may inhibit this transition.

We have developed a unified free-energy model for hydrogen by first considering two limits in the phase diagram, namely, a domain of low densities and temperatures, where only neutral species are found ( $H$  and  $H_2$ ), and a high-temperature and/or high-density domain, where ionization takes place. This paper describes the former model and focuses on the phenomenon of pressure dissociation; we will discuss the problem of pressure and temperature ionization in a future companion paper. We have not extended our calculations in the domain where solid metallic hydrogen may exist. The structure of the paper is as follows. In the next section, we discuss briefly the so-called physical and chemical pictures and give an overview of our free-energy model for the  $H$ - $H_2$  mixture. Each contribution to this free-energy model is discussed

in turn in Secs. III–V. The model is summarized in Sec. VI where we describe the computation of the chemical equilibrium between  $H_2$  and  $H$ . Comparison with experimental results and the analysis of the results will be done, respectively, in Secs. VII and VIII and concluding remarks are in Sec. IX.

## II. GENERAL CONSIDERATIONS

### A. Chemical picture and the factorization of the internal partition function

Equation-of-state models can be divided into two broad categories. In the *physical picture*, [14,15] only “fundamental” particles are considered (electrons and nuclei), which interact through Coulomb potentials. In principle, one would like to solve the Schrödinger equation for the system with quantum-statistical many-body theory, obtaining a spectrum of bound electronic states, forming “atoms” and “molecules” with density-dependent eigenvalues, together with free electronic states. This approach is appealing since it corresponds to our intuitive conception of the actual behavior of matter and is also formally exact. In regimes where bound states occur, the physical picture involves the Planck-Larkin formalism, which arises from a high-temperature expansion of the Coulomb interactions. This approach has been applied to partially ionized plasmas up to  $\Gamma=1$ , where  $\Gamma$  is the plasma coupling parameter [14]. Even though the physical picture probably offers the most rigorous treatment, the calculation of an EOS for the study of pressure ionization with these theories is a formidably complex problem and to our knowledge, it has not been applied at the lower temperatures relevant to this phenomenon.

On the other hand, the *chemical picture* [16–19] assumes that bound configurations, like atoms and molecules, retain a definite “identity,” and interact through pair potentials. This approach has a serious drawback. At densities corresponding to pressure ionization, the electrons in bound configurations become delocalized, bound species lose their identity, and pair potentials become meaningless [20]. Both descriptions give the same excellent results at low density or at high temperature [21], where interparticle correlations are small and in the fully ionized regime, where the distinction becomes irrelevant. In view of the practical limitations of the physical picture, the chemical picture emerges as the simpler practical alternative.

Within the framework of the chemical picture, our EOS model is based on the free-energy minimization technique [16]. The approach is particularly simple. Given a mathematical model for the Helmholtz free energy of the system as a function of total volume, temperature, and particle numbers,  $F(V, T, \{N_i\})$ , the chemical equilibrium of the mixture is obtained by minimizing  $F$  at fixed  $V$  and  $T$ , subject to the stoichiometric constraints imposed by the chemical reactions taking place in the system. Contrary to expansion techniques, contributions with strongly nonlinear dependence on density or temperature can be included with no additional effort. This method, which ensures thermodynamic consistency, be-

comes truly useful when the partition function of the system is assumed to be factorizable into kinetic, internal, and configuration contributions.

### B. Free-energy model

Hydrogen molecules and atoms are the dominant species at low temperatures ( $\log_{10} T \lesssim 4$ ) and low densities ( $\log_{10} \rho \lesssim 0$ ), as shown in Fig. 1, and we consider a free-energy model for a binary mixture of H and H<sub>2</sub>. Because all particles are very nearly classical in this regime, we can factorize the partition function and treat the small quantum effects with a semiclassical approximation. If we make the additional assumption that the internal levels of atoms and molecules are only weakly affected by the presence of nearby particles (this point is developed in Sec. IV), the Helmholtz free energy separates into ideal, configurational, internal, and quantum contributions [16,18]:

$$F = F_{\text{id}} + F_{\text{conf}} + F_{\text{int}} + F_{\text{qm}} . \quad (1)$$

The first term on the right-hand side represents the purely translational degrees of freedom of the atoms and molecules, which follow a Maxwell-Boltzmann distribution of velocities. The last three contributions are discussed separately in the following sections.

### III. THE CONFIGURATION FREE ENERGY, $F_{\text{conf}}$

The configuration free energy arises from the forces between particles, described with interaction potentials. In the regime where hydrogen atoms and molecules exist in a fluid state, they behave as classical particles. It is thus appropriate to describe these interactions with classical theories, even though the interaction potentials may implicitly have a quantum-mechanical origin.

#### A. Interaction potentials

The interaction potentials are central to the concept of the chemical picture and to the computation of the configuration free energy. We have evaluated the configuration term in the context of pairwise additive potentials, which tremendously simplifies the calculation. At high densities, this approximation becomes incorrect and we must consider  $N$ -body interactions with density-dependent potentials, based on difficult quantum-mechanical simulations. Fortunately, this problem can be partly circumvented by using experimentally determined *effective* pair potentials which include many-body effects implicitly.

##### 1. The H<sub>2</sub>-H<sub>2</sub> potential

Numerous experiments on molecular hydrogen and deuterium have probed this interaction potential over a wide range of pressures and temperatures. The Young and Ross potential [4] reproduces a wide variety of experimental results. It is based on an analysis of the latest shock-compression experiments performed on fluid hydrogen and deuterium [22–24]. The Young and Ross potential is fitted to experimental data using an equation of

state based on fluid perturbation theory, assuming a spherically symmetric *pair* potential. The resulting  $\phi_{\text{H}_2\text{-H}_2}$  is especially suitable for our purposes, since shock compression achieves high-temperature and high-pressure final states ( $T \approx 7000$  K,  $P \approx 0.8$  Mbar), typical of the very regime we want to study. It also reproduces the pressure isotherms of low-temperature static compression experiments [25,26]. By construction, the many-body effects present at the highest pressures reached by the experiments are implicitly included in this *effective pair potential*. The latter is about 40% softer than the *ab initio*  $\phi_{\text{H}_2\text{-H}_2}$  potential, clearly demonstrating the importance of many-body effects at high pressures.

Recently, static compression experiments at room temperature have indicated that the Young and Ross potential may be too stiff to describe the static results [7]. The resulting effective potential, which was not available at the time we completed our work, is about 10–15% softer than the Young and Ross potential. While this does not necessarily imply that the Young and Ross potential is inappropriate at higher temperatures, we have repeated a small subset of calculations with this new potential which are presented in Sec. VIII.

The H<sub>2</sub> molecule has axial, rather than spherical symmetry, and it is justified to ask whether the use of a spherically symmetric potential is appropriate. The answer hinges on the rotational properties of the molecule, since the anisotropic potential of a free rotator can be averaged over angles to take advantage of the simplicity of spherical symmetry. The anisotropic *ab initio*  $\phi_{\text{H}_2\text{-H}_2}$  departs from spherical symmetry by about 8% [27]. In the zero-temperature molecular *solid*, this leads to hindered rotation, with the rotational degrees of freedom “freezing” at a pressure of 0.375 Mbar [28]. Monte Carlo simulations [29] indicate that the rotation temperature rises from its free-molecule value of 85 to 1257 K at a density of 0.5 g/cm<sup>3</sup> and that as the density increases, molecules stop rotating freely and oscillate around their equilibrium orientation in the crystal before complete orientational ordering occurs. Quantum Monte Carlo (MC) simulations indicate that the pressure required for rotational freezing is around 1 Mbar [30]. Recently roton modes have been observed up to pressures of 1.62 Mbar, an indication that rotation is not completely hindered at these pressures [31]. On the other hand, it appears that if hydrogen becomes a rotationally ordered solid, band overlap occurs, causing metallization [32]. If this argument is correct, H<sub>2</sub> apparently does not form a rotationally ordered solid up to the highest pressures currently achieved in the laboratory ( $\approx 2.5$  Mbar).

Clearly, the issue of the rotational state of H<sub>2</sub> molecules in the solid phase is still controversial. On the other hand, we are interested in the fluid phase, at finite temperature, where the thermal energy of the molecules is likely to be larger than the rotational barrier [4].

In addition, because the  $\phi_{\text{H}_2\text{-H}_2}$  potential was fitted to experimental data by assuming that the molecules were free rotors in the fluid phase, any effects of hindered rotation and potential asymmetry present in the data are implicitly included in the effective potential. Considering

the lack of experimental evidence for hindered rotation, we consider that the use of this spherically symmetric *effective* potential is justified, at least in the domain explored so far by experiments on fluid molecular hydrogen.

## 2. The H-H potential

Unfortunately, no similar experimental result exists for the  $\phi_{\text{H-H}_2}$  and the  $\phi_{\text{H-H}}$  potentials. The Schrödinger equation for an ensemble of four particles, two electrons in the field of two *fixed* protons, has been solved, using a large basis of wave functions [33]. Both cases where the electrons are in the single state  $S=0$  ( $^1\Sigma$  bonding orbital, leading to the formation of an  $\text{H}_2$  molecule) or the anti-bonding  $S=1$  ( $^3\Sigma$  triplet state) have been considered in the range  $1 \leq r \leq 10$  a.u. Because of the large differences between the singlet- and triplet-state potential surfaces, the spin dependence of the H-H interaction must be taken into account. Moreover, the  $^1\Sigma$  bonding potential would allow H atoms to form  $\text{H}_2$  molecules. Thus, we could only describe the system with the physical picture which is restrained to low densities and high temperatures. We avoid the complexity of the problem by using a semiclassical formalism for averaging spin-dependent interactions [34]. In this approach, the quantum-mechanical electronic spin degrees of freedom are mapped onto classical spin degrees of freedom. For hydrogen atoms, in particular, the spin averaged pair interaction potential becomes the weighted average of the singlet and triplet potential functions:

$$\phi_{\text{H-H}} = \frac{1}{4} [3\phi(^3\Sigma) + \phi(^1\Sigma)] .$$

The resulting potential does not have any bound states; the minimum of the attractive well is at  $r=6.2$  a.u. and is 20.2 K deep. As a consequence, two atoms interacting with this spin averaged potential will not bind to form a molecule. We stress that in a consistent model based on the chemical picture it is a requirement for interaction atoms to retain their identities since  $\text{H}_2$  molecules are already included in the model.

It is convenient to develop analytic fits to tabular potentials. At the high temperatures we are considering, the softness of the repulsive part of the potential must be carefully treated. We have adopted a “generalized” Morse potential of the form

$$\phi(r) = \epsilon [ \gamma e^{-2s_1(r-r^*)} - (1+\gamma) e^{-s_2(r-r^*)} + A e^{-b(r-r^*)} ] . \quad (2)$$

Note that we recover the Morse potential when  $A=0$ ,  $\gamma=1$  and  $s_1=s_2$ . All parameters in Eq. (2) are fitted to tabulated values for  $\phi(r)$ .

## 3. The H-H<sub>2</sub> potential

The H-H<sub>2</sub> potential is derived from the potential surfaces of the  $\text{H}_3$  system [35]. They are given in terms of expressions to evaluate the total energy of three H

“atoms” in any configuration, based on a calculation similar to the one described above for H-H. To obtain a spherically symmetric H-H<sub>2</sub> pair potential, we have fixed two atoms at the equilibrium distance between the nuclei of a  $\text{H}_2$  molecule and performed an angular average of the potential of the third atom and the “molecule” for various separations. After this work was completed, we became aware of more accurate methods to obtain angular averages of nonspherical potentials [36] indicating that a simple angular averaged potential is about 35% too large in the repulsive region. In our model, the angle-averaging procedure affects only the H-H<sub>2</sub> potential, which enters as one of the three contributions to  $F_{\text{conf}}$  and whose weight peaks at 50% of molecular dissociation only. Given the large uncertainty of the real behavior of the H-H<sub>2</sub> potential at high density, we assume that this imprecision in our calculations does not bear heavily on our results concerning pressure dissociation and pressure ionization. The effect of uncertainties in the potentials is estimated and discussed in Sec. VIII C.

We use the fitting formulae of Porter and Karplus [35] to compute  $\phi_{\text{H-H}_2}$  in the range  $1 \leq r \leq 4.6$  a.u. These authors warn that their Eqs. (18a) and (18b) give inaccurate results for  $r \geq 3$  a.u. This inaccuracy is rather serious, and we have therefore used the results of Kolos and Wolniewicz [33], (which these equations are meant to approximate) instead. We find that this makes a substantial difference for  $r \geq 2.5$  a.u. [37] Porter and Karplus [35] did not study the attractive part of the potential. We can get some guidance here from the use of so called “mixing rules [38],” developed to evaluate the parameters of the mixed interaction potential from those of the pure components. Experimental studies of a variety of molecular mixtures have demonstrated their validity. For the attractive well, we have

$$\epsilon_{ij} = \sqrt{\epsilon_{ii}\epsilon_{jj}} ,$$

$$r_{ij}^* = \frac{1}{2}(r_{ii}^* + r_{jj}^*) ,$$

which gives  $\epsilon_{\text{H-H}_2} = 25.5$  K and  $r_{\text{H-H}_2}^* = 6.35$  a.u.

The fitted coefficients for  $\phi_{\text{H-H}}$  and  $\phi_{\text{H-H}_2}$  are given in Table I, and all three potentials used in the actual EOS calculation are shown on Fig. 2. The final fits agree with the tabulated values to better than 10%.

Clearly, little faith can be put on these potentials at very small separations. The *ab initio* potentials were computed for  $r \geq 1.0$  a.u.; inside that value, the analytic fits are convenient extrapolations at best. The same can be said of the effective  $\text{H}_2$ - $\text{H}_2$  potential which is known experimentally down to about 2.8 a.u. When the separation between particles (or protons) becomes of the order of 1 a.u., the electronic wave functions are so distorted from their isolated forms that it is impossible to talk about “atoms” and “molecules” anymore. This is the regime where the chemical picture fails.

This lack of knowledge of the very-short-range potential is of little consequence at the temperatures and densities relevant for the H-H<sub>2</sub> binary mixture, because particles do not approach each other closely enough to be subjected to the innermost part of the potential.

TABLE I. Coefficients for  $\phi_{\text{H-H}}$  and  $\phi_{\text{H-H}_2}$  [Eq. (2)].

	H-H	H-H <sub>2</sub>
$\epsilon$ (K)	20.2	25.5
$\gamma$	0.4615	0.6
$s_1$ ( $\text{\AA}^{-1}$ )	1.6367	1.4740
$s_2$ ( $\text{\AA}^{-1}$ )	1.2041	1.4740
$r^*$ ( $\text{\AA}$ )	3.2809	3.3603
$A$	0	$1.851 \times 10^{-7}$
$b$ ( $\text{\AA}^{-1}$ )		8.2392

### B. Fluid perturbation theory

To compute the configuration free energy associated with the three interacting potentials described above, we used the well-known fluid perturbation theory, applied extensively to the study of the thermodynamic properties of liquids near melting [39]. Among all existing perturbation schemes, we elected to use the expansion Weeks-Chandler-Andersen (WCA) expansion [40], whose superiority has been assessed in numerous applications by comparison with experimental data and computer simulations [39,41]. Truncating the expansion after the first

order, we obtain the so-called ‘‘high-temperature approximation’’ (HTA) [40] to the free energy:

$$F_{\text{conf}} = F_0^N + \langle \mathcal{U}_1^N \rangle_0.$$

Here  $F_0^N$  is the free energy of the reference system and the second term (HTA) is given by

$$\langle \mathcal{U}_1^N \rangle_0 = \frac{N^2}{2V} \int \phi_1(r) g(r) d^3r, \quad (3)$$

where  $N$  is the number of particles,  $V$  the volume of the system,  $g(r)$  is the pair correlation function of the reference system, and the potential  $\phi$  is separated in reference and perturbation parts:  $\phi(r) = \phi_{\text{ref}}(r) + \phi_1(r)$ .

#### 1. Choice of a reference potential

The evaluation of the expansion, up to and including the HTA term, requires the knowledge of the free energy of the reference system and of its pair correlation function(s). The only reference system appropriate to describe molecular fluids and for which analytic expressions for the free energy as well as for the pair correlation functions exist is the hard-sphere fluid [42–44].

#### 2. Modification of the WCA theory

The configuration free energy of two-component fluid perturbation theory can be written as

$$\frac{\beta F_{\text{conf}}}{N} \equiv \frac{\beta F_{\text{HS}}}{N} + \frac{N}{2V} \sum_{i,j=1}^2 x_i x_j \int g_{ij}^{\text{HS}}(r) \beta \phi_{ij}^{\text{pert}}(r) \times d^3r + F_{\text{HO}}, \quad (4)$$

where  $\beta = 1/kT$ ,  $x_i = N_i/N$  is the number concentration of species  $i$ ,  $F_{\text{HS}}$  is the hard-sphere free energy of a binary system [42] and the second term on the right-hand side is the HTA contribution.

The last term,  $F_{\text{HO}}$  represents all the higher-order terms of the expansion, that are difficult to evaluate and which can be approximated at low density by the random-phase approximation (RPA). For reasons detailed below we have dropped this term.

The hard-sphere radii entering the calculation of  $F_{\text{HS}}$  and  $F_{\text{HTA}}$  are determined by the WCA criterion which reads, for a two-component system:

$$\sum_{i,j=1}^2 x_i x_j I_{ij} = 0 \quad i, j = 1, 2, \quad (5)$$

where  $I_{ij}$  is given by [41]

$$I_{ij} = \int_0^{\sigma_{ij}} y_{ij}^{\text{HS}}(r) \exp[-\beta \phi_{ij}^{\text{ref}}(r)] d^3r + \int_{\sigma_{ij}}^{\lambda_{ij}} g_{ij}^{\text{HS}}(r) \{ \exp[-\beta \phi_{ij}^{\text{ref}}(r)] - 1 \} d^3r. \quad (6)$$

Here the functions  $y_{ij}(r)$  are defined by  $y_{ij}(r) = g_{ij}(r) \exp[\beta \phi_{ij}(r)]$ , whereas  $\lambda_{ij}$  denotes the break point for the separation of the interaction potential  $\phi_{ij}(r)$  into reference and perturbation parts, and  $\sigma_{ij}$  stands for the corresponding hard-sphere diameter. Equation (6) does not, in general, have a unique solution for  $\{\sigma_{11}, \sigma_{12}, \sigma_{22}\}$ ,

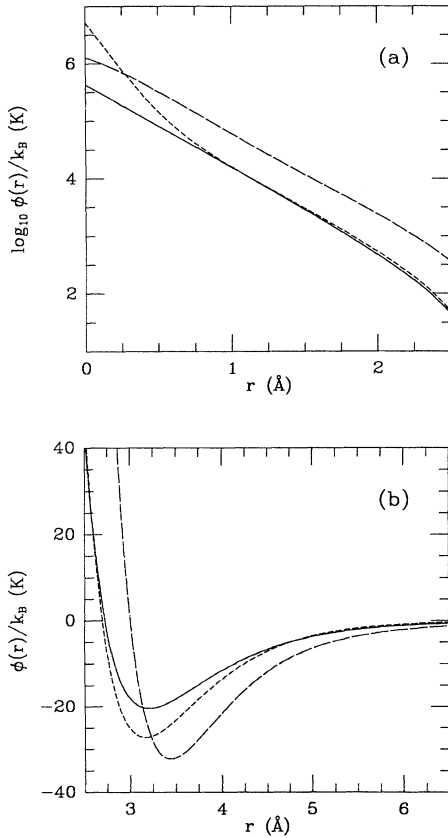


FIG. 2. H<sub>2</sub>-H<sub>2</sub>, H<sub>2</sub>-H, and H-H interaction potentials used in the EOS calculation (defined by Eq. (2) with coefficients given in Table I and Eqs. (1)–(5) of Ref. [4]). H<sub>2</sub>-H<sub>2</sub>, long dashes; H<sub>2</sub>-H, short dashes; H-H, solid line, (a) repulsive cores on a logarithmic scale. (b) Long-range attractive part on a linear scale.

thus leading to poor predictions of the pair correlation functions of the fluid [45]. On the other hand, the set of three coupled equations

$$I_{11}=0, \quad (7a)$$

$$I_{22}=0, \quad (7b)$$

$$I_{12}=0, \quad (7c)$$

does have a unique solution. The three hard-sphere diameters  $\sigma_{ij}$  entering Eq. (7) are related by the additive condition for the hard-sphere system:

$$\sigma_{12} = \frac{1}{2}(\sigma_{11} + \sigma_{22}). \quad (8)$$

We first solve Eqs. (7a) and (7b) simultaneously for  $\sigma_{11}$  and  $\sigma_{22}$ . The approximation proposed by Grundke and Henderson [44] is used for the functions  $y_{ij}^{\text{HS}}(r)$  for  $r < \sigma_{ij}$ , while the functions  $g_{ij}^{\text{HS}}(r)$  are computed in the Percus-Yevick approximation [46] with the Verlet and Weis correction [47] which brings the Percus-Yevick  $g_{ij}^{\text{HS}}(r)$  to within  $\approx 2\%$  of the computer simulations results.

Even though the WCA form of hard-sphere perturbation theory is quite successful in studies of cryogenic molecular fluids, where  $kT \approx \varepsilon$  ( $\varepsilon$  is the depth of the potential minimum [Fig. 2(b)]), it suffers from several difficulties in the high-temperature, high-density regime in which we are interested. First, the use of a hard-sphere fluid to approximate the reference potential cannot be justified *a priori* at temperatures so high that the softness of the repulsive potential becomes noticeable ( $kT/\varepsilon > 10$ ). This constitutes a serious conceptual problem in the application of hard-sphere perturbation theory. Second, at densities near the hard-sphere melting transition, the WCA criterion overestimates the hard-sphere diameter and leads to a metastable reference system. This prompted Kang *et al.* [48] to suggest a different potential separation which reduces to the WCA case at low enough densities. This scheme was further modified for binary mixtures and the validity of this latter method and of the application of fluid perturbation theory at high pressure and high temperature has been assessed by comparison with MC calculations [49]. The internal energy and pressure obtained with this modified WCA theory agree with the MC results *within less than 3%* in most cases, a factor of 4–10 improvement over the WCA results, even at high temperature ( $T = 10\,000$  K) and at high densities ( $\rho = 1$  g/cm<sup>3</sup>) where WCA gives very poor or even unphysical results.

As mentioned in Sec. III B 2, we have dropped the RPA term in writing Eq. (4). The RPA constitutes an approximation to the higher-order terms which is useful when the perturbation is weak and the density is low. If these conditions are not met, the RPA term diverges, a situation usually associated with a phase transition in simple systems (the so-called ‘‘RPA catastrophe’’). With the potential separations we have considered, the conditions of validity of the RPA are violated at densities well below those where a RPA catastrophe could be associated with any expected critical phenomenon. Since we find that Eq. (4) gives a good description of the thermodynamics of our binary mixture *when using appropriate potential*

*separations*, we conclude that the higher-order terms of the perturbation expansion are small and that the relatively large RPA term is a very poor approximation of these terms and must therefore be ignored.

In this section we have pointed out that it is possible to use fluid perturbation theory based on a hard-sphere reference system and the HTA approximation to compute the thermodynamics of a high-temperature binary mixture with good accuracy, provided that particular care is taken in choosing the separation of the interaction potentials into reference and perturbation parts. Comparison with MC simulations shows that our scheme gives a good description of the configuration term for a mixture of hydrogen atoms and molecules over the full range of temperatures and densities of interest. We stress that the hard-sphere diameters  $\sigma_{ij}$  which characterize the interactions in the H-H<sub>2</sub> mixture are determined thermodynamically by application of the WCA criterion. As a consequence, the  $\sigma_{ij}$  are temperature and density dependent, leading to an implicit dependence of the configuration energy on  $\rho$  and  $T$ .

#### IV. BOUND STATES AND THE INTERNAL FREE ENERGY, $F_{\text{int}}$

The contributions of the bound states of atomic and molecular hydrogen are given by

$$\begin{aligned} F_{\text{int}} &= -kT \sum_{i=1}^2 N_i \ln Z_i \\ &= -kT \sum_{i=1}^2 N_i \ln \sum_{\alpha} g_{i\alpha} e^{-\beta \varepsilon_{i\alpha}}, \end{aligned} \quad (9)$$

where  $\alpha$  runs over all bound states of species  $i$ , and  $g_{i\alpha}$  and  $\varepsilon_{i\alpha}$  are the multiplicity and the eigenenergy of state  $\alpha$ , respectively. In the case of isolated atoms, Eq. (9) leads to a divergent partition function  $Z_i$ , as the sum over  $\alpha$  involves an infinite number of terms which increases monotonically for large  $\alpha$ . This difficulty is usually alleviated by recalling that no particle is truly isolated and that interactions with other particles provide a form of cutoff in the sum over states, introducing a density dependence in  $Z_i$ . This section is devoted to the effect of neighboring particles on the internal partition function of bound species, which is a key problem when treating pressure ionization. In the context of the H-H<sub>2</sub> model, it is interesting to inquire whether particle interactions induce pressure dissociation of the molecules prior to pressure ionization.

##### A. The occupation probability formalism

The close relationship between the density dependence of the partition function and the interparticle interactions has not always been appreciated in previous work, sometimes resulting in gross statistical-mechanical inconsistencies in the free-energy model. Recently, Hummer and Mihalas [17] (hereafter, HM) have developed an *occupation probability formalism* which formally guarantees statistical-mechanical consistency between the description of interactions and the internal partition function (IPF) in the model for the free energy.

Consider a one-component system with a nonideal free

energy  $f$  which depends on the population of each bound state,  $N_\alpha$ . Its free energy is

$$F = F_{\text{id}} - NkT \ln Z + f,$$

where  $N = \sum_\alpha N_\alpha$  and  $Z = \sum_\alpha g_\alpha \exp(-\beta \epsilon_\alpha)$ . This free energy can be rewritten as [17,50,51]

$$F = F_{\text{id}} - NkT \ln \tilde{Z} + f - \sum_\alpha N_\alpha \frac{\partial f}{\partial N_\alpha}, \quad (10)$$

where  $\tilde{Z}$  is a modified partition function

$$\tilde{Z} = \sum_\alpha \omega_\alpha g_\alpha e^{-\beta \epsilon_\alpha},$$

and the occupation probability  $\omega_\alpha$  of state  $\alpha$  is defined by

$$\omega_\alpha = \exp \left[ -\beta \frac{\partial f}{\partial N_\alpha} \right]. \quad (11)$$

The fractional population of state  $\alpha$  will be given by

$$N_\alpha / N = \omega_\alpha g_\alpha e^{-\beta \epsilon_\alpha} / \tilde{Z}. \quad (12)$$

The occupation probability measures the probability that a state identical to a level of an isolated atom can actually exist in the midst of perturbations by neighboring particles. It expresses the reduction in phase space available to the state. It is computed self-consistently with the nonideal term; that is, the effect working *inside* bound particles is consistent with the *outside* interactions. The last term on the right-hand side of Eq. (10) has often been ignored in previous work, but it is required to ensure statistical-mechanical consistency. Note, in particular, that if  $f$  is linear in  $N_\alpha$ , the last two terms of Eq. (10) cancel and the nonideal term has been entirely absorbed in the occupation probability,  $\omega_\alpha$ . In this case, the total free energy is no longer explicitly dependent on the population of each excited level ( $N_\alpha$ ) and the internal free energy reads

$$\begin{aligned} F_{\text{int}} &= -kT \sum_{i=1}^2 N_i \ln \tilde{Z}_i \\ &= -kT \sum_{i=1}^2 N_i \ln \sum_\alpha \omega_{i\alpha} g_{i\alpha} e^{-\beta \epsilon_{i\alpha}}. \end{aligned} \quad (13)$$

This formalism offers a number of advantages over work which relies on *ad hoc* cutoff procedures for the IPF, or even on more sophisticated models where an attempt is made to provide qualitative consistency between the perturbed internal states and the nature of the interactions (for example, using hard-sphere interaction and the confined atom model for the internal states). In particular, for any reasonable form of interaction  $f$ , the  $\omega_\alpha$  decrease fast enough with  $\alpha$  to ensure convergence of the partition function as the strength of the interaction increases. By construction, the  $\omega_\alpha$  are smooth, monotonic, and continuous functions of  $\rho$  and  $T$ , causing states to disappear *gradually* from the partition function sum. This preserves the continuity of the free energy and its derivatives, avoiding the discontinuities that appear in models in which states are lost in discrete steps. Due to the probabilistic interpretation of the occupation proba-

bility, it is a simple matter to account for a number of independent interactions. This formalism provides a *physically plausible description* of pressure dissociation and ionization.

Physically, we expect that as the density is raised, not only do states disappear from the IPF, but also their eigenenergy must shift towards the continuum of unbound states. The occupation probability formalism does not involve such level shifts. Instead, it uses the eigenvalues of the isolated particle, simplifying tremendously the task of evaluating the IPF. Is this a reasonable description of the internal structure of bound species interacting with their neighbors? The equation of state is not sensitive enough to the details of the internal structure of bound species to provide a good diagnostic of various choices for the  $\omega_\alpha$  and the energy eigenvalues of the states. On the other hand, spectroscopic experiments probe the internal levels directly. Here, we depart temporarily from our H-H<sub>2</sub> model to discuss spectroscopic experiments on plasmas. This is not directly relevant to the "neutral model" but it illustrates the point clearly.

In these experiments, one observes the emission line spectrum of a relatively dense plasma. Nonideal effects, screening effects in the plasma, and the Stark effect broaden and shift the lines and introduce asymmetries into the line profiles. The pressure shifts observed experimentally for hydrogen and hydrogenic ions are very small [52,53] even at electronic densities as large as  $N_e/V \approx 10^{21} \text{ cm}^{-3}$  [54]: typically,  $\delta\lambda/\lambda \lesssim 3 \times 10^{-4}$ . Such small shifts are entirely negligible in an EOS calculation.

In support of the HM formalism, a direct comparison with measurements of the emissivity of a  $T = 1.1 \times 10^4 \text{ K}$  hydrogen plasma at electronic densities up to  $N_e = 10^{17} \text{ cm}^{-3}$  [52] is possible. The simulation of the emissivity based on the occupation probability formalism agrees beautifully with the experimental result [55]. It is of course possible that the agreement will deteriorate when similar experiments are performed with denser plasmas.

It must be pointed out that a substantial dependence of the internal structure on the interparticle interactions effectively precludes the factorization of the configuration and internal contributions from the total partition function, requiring instead that the two be computed in a self-consistent manner. In view of the experimental evidence and of the lack of a reliable theory to compute the energy level shifts—which must occur at very high densities—self-consistently with the interactions, the use of unperturbed energy levels in the occupation probability formalism is justified at low densities (say,  $\log_{10} \rho \lesssim -2$ ) and seems reasonable at higher densities.

There is evidence that the heuristic occupation probability formalism, with its assumptions and slight inconsistencies which arise in practical applications, does provide a quantitatively correct EOS. Oscillation spectra of solar models computed with an EOS based on this formalism show a much improved agreement with the observed frequencies than had been obtained previously [9]. Also, a comparison of equations of state for a hydrogen and helium mixture under conditions found in the solar interior based on (1) the chemical picture and the occupation probability formalism and (2) an entirely indepen-

dent method based on the physical picture, shows a nearly perfect agreement in the second derivatives of the free energy [21], which are notoriously sensitive on details of the model.

We have elected not to use the so-called Planck-Larkin (PL) partition function which has been employed in both the physical and chemical pictures for equations of state of partially ionized plasmas. The PL function arises naturally in the physical picture as a cancellation between scattering states and highly excited states in the two-body interaction term (second coefficient in the virial expansion). Application of the PL partition function leads to a nicely convergent sum in Eq. (9). When applied to  $F_{\text{int}}$  in a model based on the chemical picture and the factorization of the partition function [Eq. (1)], the PL partition function can be formally interpreted as an occupation probability [55]. However, the resulting level occupations fail to reproduce the experimental emissivity data of Ref. [52], as demonstrated in Ref. [55]. As a consequence, it would be incorrect to use the PL partition function in the context of our free-energy model. We stress that this does not preclude applying the PL partition function in the physical picture [56].

How do we actually compute the occupation probabilities for the mixture of hydrogen atoms and molecules? To simplify the notation, consider a one-component system. Exploiting the nature of interatomic potentials, HM use an excluded-volume interaction to represent the strong repulsive cores, which represent the main features of these potentials. Their configuration free energy is [17]

$$F_{\text{conf}} = \frac{\pi k T}{12V} \sum_{\alpha, \alpha'} N_{\alpha} N_{\alpha'} (\sigma_{\alpha} + \sigma_{\alpha'})^3, \quad (14)$$

where  $\sigma_{\alpha}$  is the hard-sphere diameter corresponding to state  $\alpha$ . Equation (14) can be compared to our expression for  $F_{\text{conf}}$  given by Eq. (4). Remember that the configuration term must depend on the level populations ( $N_{\alpha}$ ) to provide dissolution of states described by the occupation probability. As we shall see below, Eq. (14) represents the lowest-order approximation (first order in packing fraction) to the hard-sphere fluid free energy entering Eq. (4). At the relatively low densities to which Hummer and Mihalas [17] limit their study ( $\rho \leq 10^{-2} \text{ g cm}^{-3}$ ), this is a reasonable choice for  $F_{\text{conf}}$ . It has the advantage of being easily linearized by invoking a low excitation approximation (see below). This issue is important since in practice, this formalism is useful only when  $E_{\text{conf}}$  is linear in the level populations, leading to cancellation of the last two terms in Eq. (10). Otherwise, the total free energy retains an explicit dependence on the  $N_{\alpha}$ , and the free-energy minimization must be performed with respect to the populations of all levels of all species. Solving the chemical equilibrium of such a large number of species would be computationally prohibitive.

Our choice of  $F_{\text{conf}}$  aims at describing the nonideal physics of the dense fluid and is accordingly a much more complicated function of density than Eq. (14). It exhibits strongly nonlinear behavior, except at very low densities. It must also be realized that the interaction potentials de-

scribed in Sec. III A apply to atoms and molecules in their ground state. Data on excited atomic or molecular potentials of the nature required for our calculation is virtually nonexistent. As a consequence, it is not possible to include the HTA term in the calculation of the occupation probability. It is possible, however, to relate our  $F_{\text{conf}}$  to the HM formalism by modifying it slightly and introducing an additional approximation. In essence, we use the same expression for the occupation probability as Ref. [17], while keeping the nonlinear part of Eq. (4) intact. This comes at the price of a small inconsistency in the model, as discussed below.

The linear term in the expansion of  $F_{\text{HS}}$  in powers of the packing fraction  $\eta$  is exactly the excluded volume free energy, that is

$$(4 - 3y_1)\eta = \frac{\pi}{12NV} \sum_{i,j=1}^m N_i N_j (\sigma_i + \sigma_j)^3,$$

where  $y_1$  is defined in Ref. [42].

The configuration free energy given by Eq. (4) accounts only for interactions between particles in their ground state. To obtain occupation probabilities for excited states and the desired density-dependent cutoff in the sum over states in the IPF, we modify  $F_{\text{conf}}$ , but *only in the term of the hard-sphere free energy* ( $F_{\text{HS}}$ ) which is linear in  $\eta$ . The remaining, nonlinear, terms in  $F_{\text{conf}}$  are evaluated as if all particles were in their ground states. The nonideal free energy now reads

$$F_{\text{conf}} = \frac{\pi k T}{12V} \sum_{i,j,\alpha,\alpha'} N_{i\alpha} N_{j\alpha'} (\sigma_{i\alpha} + \sigma_{j\alpha'})^3 \quad (15a)$$

$$- NkT(4 - 3y_1)\eta \quad (15b)$$

$$+ F_{\text{HS}} \quad (15c)$$

$$+ \frac{1}{2V} \sum_{i,j} N_i N_j \int g_{ij}^{\text{HS}}(r) \phi_{ij}^{\text{pert}}(r) d^3r. \quad (15d)$$

Expressions for  $F_{\text{HS}}$ ,  $y_1$ , and  $\eta$  are given in Ref. [42]. Latin indices ( $i, j$ ) represent the different species of the mixture while greek indices ( $\alpha, \alpha'$ ) label their internal levels. The last three terms on the right-hand side depend only on  $N_i$ , the total population of species  $i$ , summed over all internal states. They can only affect the relative populations of the species (in chemical equilibrium), not the internal partition functions. The second term [Eq. (15b)] is introduced to avoid double counting of the term linear in  $\eta$  between Eqs. (15a) and (15c). The cancellation is not exact, since it assigns ground-state diameters to all particles.

The  $N_{i,\alpha}$  dependence of  $F_{\text{conf}}$  is still quadratic [Eq. (15a)]. We linearize this term by invoking a low-excitation approximation [17], in which a particle in a given state ( $i, \alpha$ ) interacts with neighbors which are assumed to be all in their ground states ( $\alpha' = 1$ ). In this approximation, the first term on the right-hand side of Eq. (15) becomes

$$\frac{\pi kT}{12V} \sum_{i,j,\alpha,\alpha'} N_{i\alpha} N_{j\alpha'} (\sigma_{i\alpha} + \sigma_{j\alpha'})^3$$

$$\approx \frac{\pi kT}{12V} \sum_{i,j,\alpha} N_j N_{i\alpha} (\sigma_{j1} + \sigma_{i\alpha})^3,$$

and the occupation probability of level  $\alpha$  of species  $i$  is

$$\omega_{i\alpha} = \exp \left[ \frac{-\pi}{12V} \sum_j N_j (\sigma_{j1} + \sigma_{i\alpha})^3 \right]. \quad (16)$$

The validity of this approximation can be demonstrated *a posteriori*. Table IX, which is discussed in detail in Secs. VIII C and VIII D indicate that the degree of excitation of H atoms remains extremely low at the temperatures considered here. In the case of the H<sub>2</sub> molecule, the degree of electronic excitation is more relevant than the vibrational excitation reported in Table IX, simply because  $\alpha_{i\alpha}$  depends weakly on the vibration level, while it increases rapidly when electrons are promoted to higher levels (see Sec. IV B). Electronic excitation of H<sub>2</sub> is even less pronounced than for the H atom, due to a higher first excitation energy (11.4 eV compared to 10.2 eV).

As discussed in Ref. [17], the argument of the exponential in Eq. (16) is uncertain by a factor of 2, an inconsistency inherent to the linearization procedure. Because the excitation remains low throughout the temperature domain of interest, this problem is not severe. Most particles are in their electronic ground states whose population is not only affected by the somewhat erroneous  $\omega_{i1}$ , but also by the nonlinear terms represented by Eqs. (15a)–(15c) which dominate at the high densities where  $\omega_{i1}$  departs significantly from unity (see Sec. VIII D).

Equation (16) shows another interesting property of the occupation probability formalism which allows the attribution of a different radius for each state, resulting in an *individualized state-by-state cutoff* as the strength of the interaction increases. In particular, high lying states are destroyed first, as expected.

Our application of the HM formalism aims at ensuring *statistical-mechanical consistency between nonideal effects and the internal levels of bound species*. However this formalism is truly useful only when  $F_{\text{conf}}$  is linearized in terms of the level populations, thus limiting the physical content of the occupation probability to rather elementary interactions: in this case, an excluded volume treatment. As a consequence, the dissolution of states as given by the  $\omega_{i\alpha}$  will not be as efficient as the strength of the nonlinear interactions ( $F_{\text{conf}}$ ) would indicate. There is thus a continuing need for a better description of the relation between interparticle forces and internal levels of bound species.

## B. Internal levels of atoms and molecules

In the occupation probability formalism, the hard-sphere diameters are arbitrary. While HM [57] use reasonable physical arguments to estimate their hard-sphere diameters, the relation we have established between our choice of  $F_{\text{conf}}$  and the occupation probability yields the ground-state values naturally. These  $\sigma_{i1}$  are

based on a thermodynamic criterion (WCA) and are temperature and density dependent (see Sec. III B 2). For the diameters of excited states, we have used simple scaling laws based on basic results of quantum mechanics. The case of atomic hydrogen, for example, is relatively simple. For the “size” of an excited state, we propose to use the exact result of quantum mechanics for the electronic wave function. Using the expectation value of  $r$  for a state with quantum numbers  $n$  averaged over the degenerate  $l$  values [58], we obtain

$$\sigma_n = \frac{\sigma_H}{6} (5n^2 + 1), \quad (17)$$

which is normalized so that the ground state diameter is  $\sigma_H$ , the WCA diameter for H.

The IPF of atomic hydrogen reads

$$\tilde{Z}_H = 4 \sum_{n=1}^{\infty} n^2 \omega_n e^{-\beta h c (127\,736.3 - 109\,677.6/n^2)},$$

where

$$\omega_n = \exp \left[ \frac{-\pi}{12V} \sum_{i=1}^2 N_i (\sigma_n + \sigma_{i1})^3 \right], \quad (18)$$

$h$  is the Planck constant,  $c$  is the speed of light, and  $\sigma_n$  is given by Eq. (17). The energy levels are measured relative to the ( $n=0, J=0$ ) ground state of the H<sub>2</sub> molecule [59].

To determine the size of a molecular state, we again estimate the spatial extent of the electronic wave function. As the latter is rather complex, we have used the linear combination of atomic orbitals (LCAO) method, which gives reasonable values of energies and bond lengths for diatomic molecules (H<sub>2</sub> is a textbook example). We approximate the electronic wave function of the molecule by the LCAO wave function corresponding to the spectroscopic “terms” of that state. The “radius” of the molecule is defined as

$$\bar{r} = \frac{1}{2} (\bar{r}_1 + \bar{r}_2 + \bar{r}_{\text{nuc}}),$$

where  $\bar{r}_1$  and  $\bar{r}_2$  are the hydrogenic LCAO orbital radii for atoms 1 and 2, respectively, and  $\bar{r}_{\text{nuc}}$  is the internuclear separation. The latter can be found in the literature [60]. The hard-sphere diameter assigned to state  $\alpha$  with vibrational quantum number  $n$  is

$$\sigma_{\alpha n} = \frac{\sigma_{H_2}}{2.42} \left[ \bar{r}_{1\alpha} + \bar{r}_{2\alpha} + \bar{r}_{\text{eq},\alpha} \right. \\ \left. + \left[ \frac{\hbar}{\pi m_{\text{H}} c} \frac{n + \frac{1}{2}}{W_e - W_e X_e (n + \frac{1}{2})} \right]^{1/2} \right] \text{Å}, \quad (19)$$

where  $\bar{r}_{\text{eq},\alpha}$  is the equilibrium nuclear separation and 2.42 Å normalizes Eq. (19) so that  $\sigma_{10} = \sigma_{H_2}$ , and  $\sigma_{H_2}$  is the WCA diameter of H<sub>2</sub>. The last term on the right-hand side of Eq. (19) is a correction for nuclear vibrational motion,  $W_e$  and  $W_e X_e$  being vibrational spectroscopic constants and  $m_{\text{H}}$  is the mass of the H atom.

We have discussed the possibility of hindered rotation at high densities. Recently, a decrease in the vibration frequency of H<sub>2</sub> molecules at pressures above 1 Mbar has been measured [5]. In the conditions of interest for this model, this frequency drop is less than 4%, and the net effect on the EOS is only a fraction of a percent, and we neglected it altogether. The effect of this vibron softening on pressure ionization is discussed in paper II.

Molecular hydrogen has 46 bound states, each with vibrational and rotational sublevels. The energy of state  $\alpha$  with vibrational number  $n$  and rotational number  $J$  is calculated from [60]

$$\begin{aligned} \varepsilon(\alpha, n, J) = & T_e(\alpha) + W_e(\alpha)(n + \frac{1}{2}) - W_e X_e(\alpha)(n + \frac{1}{2})^2 \\ & + B_e(\alpha)J(J+1) - D_e(\alpha)J^2(J+1)^2 \\ & - \alpha_e(\alpha)(n + \frac{1}{2})J(J+1) - 2170.3 \text{ cm}^{-1}, \end{aligned} \quad (20)$$

The constant 2170.3 cm<sup>-1</sup> is introduced to make  $\varepsilon(1,0,0)$  coincident with the ground state of the molecule. This expression includes anharmonicity corrections, deviations from the rigid rotator approximation, and vibration-rotation coupling [61]. The various constants  $T_e$ ,  $W_e$ ,  $W_e X_e$ ,  $B_e$ ,  $D_e$ , and  $\alpha_e$  for each electronic state are taken from Ref. [60].

Since H<sub>2</sub> is a homonuclear molecule, the total wave function of the nuclei must be antisymmetric under exchange of the two protons. Ortho-hydrogen ( $S_{\text{nuc}}=1$ ) has odd  $J$  values only and para-hydrogen ( $S_{\text{nuc}}=0$ ) has even  $J$  values only, for  $\Sigma_g, \Pi_g, \Delta_g, \dots$  states, and vice versa for the  $\Sigma_u, \Pi_u, \Delta_u$  states. The adopted multiplicities  $g'$  are given in Table II.

Finally, the molecular partition function reads

$$\begin{aligned} \tilde{Z}_{\text{H}_2} = & \sum_{\alpha=1}^{46} \sum_{n=0}^{n_{\text{max}}(\alpha)} \sum_{J=0}^{J_{\text{max}}(n,\alpha)} g'(2S+1)(2J+1) \\ & \times \omega_{\alpha n} e^{-\beta\varepsilon(\alpha,n,J)}, \end{aligned} \quad (21)$$

where  $\varepsilon(\alpha, n, J)$  is given by Eq. (20). The occupation probability is

$$\omega_{\alpha n} = \exp \left[ \frac{-\pi}{12V} \sum_{i=1}^2 N_i (\sigma_{i1} + \sigma_{\alpha n})^3 \right], \quad (22)$$

where  $\sigma_{\alpha n}$  is given by Eq. (19).

We emphasize that the  $\omega_{\alpha}$  depend on the density but

TABLE II. Multiplicity  $g'$  for the H<sub>2</sub> molecule. For  $\Lambda \neq 0$  states, the assumed degeneracy of even and odd symmetry states implies  $g'=4$ .

State	$J$	$g'$	$S_{\text{nuc}}$	
$\Sigma_g$	odd	3	1	ortho-H <sub>2</sub>
$\Sigma_g$	even	1	0	para-H <sub>2</sub>
$\Sigma_u$	odd	1	0	para-H <sub>2</sub>
$\Sigma_u$	even	3	1	ortho-H <sub>2</sub>
$\Pi, \Delta$	all	4		

also on the temperature through the hard-sphere diameters  $\sigma_{ij}$ .

## V. THE QUANTUM CORRECTION, $F_{qm}$

It is possible to account for weak quantum effects due to the finite size of the particles by using the semiclassical approximation when taking the trace of the Hamiltonian. This leads to the well-known  $\hbar^2$  expansion of the free energy [62]. The first nonvanishing term of the expansion reads

$$F_{qm} = \frac{\pi \hbar^2}{12kTV} \sum_{i,j} \frac{N_i N_j}{m_{ij}} \int \nabla^2 \phi_{ij} g_{ij}(r) r^2 dr, \quad (23)$$

where

$$m_{ij} = \frac{m_i m_j}{m_i + m_j}$$

is the reduced mass of particles of types  $i$  and  $j$ .

## VI. COMPUTATION OF THE CHEMICAL EQUILIBRIUM

We now summarize the main assumptions and approximations of our model free energy for a mixture of hydrogen atoms and molecules.

(1) The model is based on the chemical picture and we assume factorizability of the partition function and classical particle statistics.

(2) We account for weak quantum diffraction effects with the Wigner-Kirkwood  $\hbar^2$  correction.

(3a) The configuration free energy is evaluated in the framework of the WCA fluid perturbation theory in the HTA approximation, after suitable modification for application to a binary mixture at high densities and temperatures. We consider only pairwise interactions.

(3b) We use an experimental H<sub>2</sub>-H<sub>2</sub> potential, and *ab initio* H-H<sub>2</sub> and H-H potentials. The latter results from a simple averaging of the bonding and antibonding H-H potentials and cannot sustain bound states.

(4a) The energies of bound levels are those of the isolated atom or molecule and the effect of interparticle interactions is described with an occupation probability formalism.

(4b) Occupation probabilities are computed from the lowest order, excluded volume part of the configuration free energy.

(4c) The ground-state hard-sphere diameters are formally given by the WCA criterion and are temperature and density dependent. Diameters for excited states are obtained by simple scaling laws.

(4d) The practical realization of the occupation probability formalism requires the linearization of the excluded volume interaction (the low excitation approximation). Bringing all contributions to our free-energy model together, we obtain

$$\begin{aligned}
\frac{\beta F}{N} = & \sum_{i=1}^2 x_i \left[ \ln \frac{N_i}{V} \left[ \frac{2\pi\hbar^2}{m_i kT} \right]^{3/2} - 1 \right] - \sum_{i=1}^2 x_i \ln \sum_{\alpha} g_{i\alpha} \omega_{i\alpha} e^{-\beta \epsilon_{i\alpha}} + [\beta F_{\text{HS}}(N_1, N_2, \sigma_1, \sigma_2, V, T) / N - (4 - 3y_1)\eta] \\
& + \frac{N}{2V} \sum_{i,j=1}^2 x_i x_j \int \beta \phi_{ij}^{\text{pert}}(r) g_{ij}^{\text{HS}}(N_1/V, N_2/V, \sigma_1, \sigma_2, r) d^3r \\
& + \frac{\hbar^2}{48(kT)^2} \frac{N}{V} \sum_{i,j=1}^2 \frac{x_i x_j}{m_{ij}} \int \nabla^2 \phi_{ij}(r) g_{ij}^{\text{HS}}(N_1/V, N_2/V, \sigma_1, \sigma_2, r) d^3r, \tag{24}
\end{aligned}$$

where  $m_i$  is the mass of particles of species  $i$ , and  $\omega_{i\alpha}$  is the occupation probability of level  $\alpha$  of species  $i$ , as defined by Eqs. (18) and (22). The summation index  $i$  labels the species and we identify atoms (H) as  $i=1$  and molecules ( $\text{H}_2$ ) as  $i=2$ . The first term on the right-hand side (rhs) is the translational, Maxwell-Boltzmann free energy. The third term on the rhs is the nonlinear contribution of the hard-sphere reference fluid, the linear part being absorbed in the internal structure (second term on the rhs). The perturbation potential  $\phi_{ij}^{\text{pert}}(r)$ , is defined by Eqs. (1)–(5) of Ref. 4 and Eq. (2) and by the potential separations discussed in Ref. [53] and  $g_{ij}^{\text{HS}}(N_1/V, N_2/V, \sigma_1, \sigma_2, r)$  is the pair correlation function of the hard-sphere fluid. All other symbols have been defined previously. The concentrations of each species are imposed by the conditions of chemical equilibrium and are constrained by  $x_1 + x_2 = 1$ .

This free-energy model has three independent variables, which we have chosen as  $x_1$ ,  $T$  and the mass density  $\rho$ . Once the three independent variables are fixed, we first solve Eqs. (7a) and (7b) for  $\sigma_1$  and  $\sigma_2$ , then  $\sigma_{12}$  follows by Eq. (8). Solving Eq. (7c) gives the proper form of the potential separation for  $\phi_{12}(r)$ . Each term of Eq. (24) can then be evaluated to obtain the total free energy.

The chemical equilibrium is given by the condition

$$\delta F = \left. \frac{\partial F}{\partial N_{\text{H}}} \right|_{N_{\text{H}_2}, V, T} dN_{\text{H}} + \left. \frac{\partial F}{\partial N_{\text{H}_2}} \right|_{N_{\text{H}}, V, T} dN_{\text{H}_2} = 0,$$

where the changes in particle number are related by the stoichiometric coefficients of the chemical reaction:  $dN_{\text{H}} = -2dN_{\text{H}_2}$ .

In a chemical equilibrium calculation,  $N$  is not constant in general, but the total amount of matter involved does not change. Then it is more appropriate to choose the free energy per gram, or equivalently, the free energy per proton, as the quantity to be minimized. The independent variables of the specific free energy are  $(x_1, \rho, T)$ , in terms of which the condition for equilibrium can be written as

$$\left. \frac{\partial \bar{F}}{\partial x_1} \right|_{\rho, T} = 0. \tag{25}$$

We have used a robust algorithm for locating the minimum of a function without using its derivative known as Brent's method [63]. The minimization algorithm is stopped when it has found the minimum free energy to within one part in  $5 \times 10^{12}$ . Because  $\bar{F}$  has a

“broad” minimum, we prefer to specify the convergence criterion on  $\bar{F}$  rather than on  $x_1$ . The corresponding uncertainty on  $x_1$  is about  $10^{-7}$ . For a representative selection of  $(\rho, T)$  points, we have verified that our free-energy model has a single minimum. This ensures that Eq. (25) has only one solution.

## VII. COMPARISON WITH EXPERIMENTAL RESULTS

We assess the reliability of our model by comparing the predicted thermodynamics with experimental results. Unfortunately, the data available in this regime is limited to a static compression isotherm at room temperature and shock compression experiments.

Figure 3 shows the 300-K pressure isotherm up to the solidification point (about  $5.4 \times 10^{10}$  dyn/cm<sup>2</sup>). Under these conditions, the fluid is purely molecular. Our  $P$ - $V$

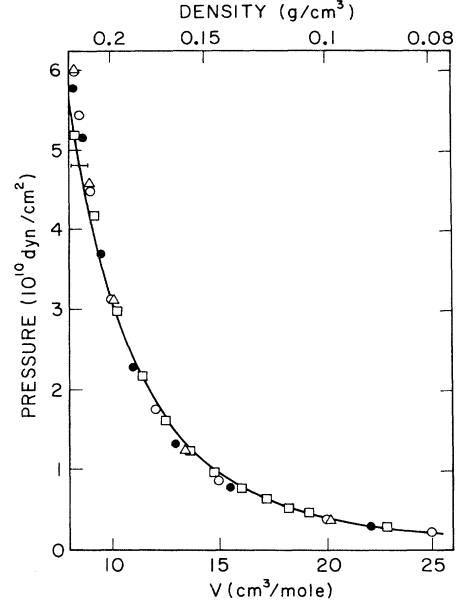


FIG. 3. 300-K pressure isotherm of fluid molecular hydrogen. The solid curve represents experimental data (Ref. [26]). Theoretical calculations are shown by various symbols: Ref. [4], open circles; the SESAME EOS library No. 5251 (hydrogen: Ref. [68], squares); Ref. [69], (triangles); and this calculation (solid circles). Experimental uncertainties are reflected in the  $\text{H}_2$ - $\text{H}_2$  potential used in all but the SESAME calculation. The magnitude of this uncertainty in the theoretical compression curves is shown by the error bar.

relation (solid circles) is in excellent agreement with the calculation presented in Ref. 4 (open circles). Comparison with the pressure, density, and packing fraction of the fluid along the melting curve calculated by these authors again shows excellent agreement. Our computations also reproduce the experimental data [26] quite well, (solid curve in Fig. 3). The exception to this is the region  $V < 10 \text{ cm}^3/\text{mol}$ , where both our calculation and that of Ref. [4] yield too high a pressure. This is probably due to the uncertainty inherent in the theoretical calculation, where a 4% uncertainty in the predicted volume arises from the large volumetric error bars in the experimental data (both shock tube and diamond anvil experiments) used to fit the effective pair potential [4]. This uncertainty is shown by the error bar in Fig. 3. This excellent agreement with both Ref. [4] and the experimental results is not surprising since we use the same  $\text{H}_2\text{-H}_2$  interaction potential which was constructed to fit a broad set of experimental results. It indicates, however, that the differences between the two models are inconsequential at this low temperature.

The most constraining data come from the high temperatures and pressures achieved in shock compression experiments, where the compression curve ( $P, V$ ) of the sample follows a ‘‘Hugoniot curve’’. Using the Rankine-Hugoniot jump conditions across the shock front, one obtains the Hugoniot relations [64]. Only one of these is of interest to us:

$$U - U_0 = \frac{1}{2}(P + P_0)(V_0 - V),$$

which simply reflects the law of energy conservation. Here  $V$ ,  $P$ , and  $U$  represent the specific volume of the sample, the pressure and the specific internal energy, respectively. The subscript 0 refers to the initial state (in front of the shock). The single-shock Hugoniot curve for hydrogen is shown in Fig. 4, with points along the theoretical curve given in Table III. Double-shock experiments have been performed on deuterium ( $\text{D}_2$ ), but not on  $\text{H}_2$ . Since the high compression reached in these experiments constitutes an important test of our model, we have also generated Hugoniot curves for  $\text{D}_2$ . The model is easily adapted to this case by changing the masses of the particles and using the appropriate spectroscopic constants and multiplicities in the IPF. The corresponding single-shock and reflected Hugoniot curves are shown along with the data in Fig. 5 and Table IV. The theoretical Hugoniot curves match the data extremely well, especially the more accurate measurements of Ref. [22] (squares). Our calculation agrees with the data as well as if not better than that of Ross, Ree, and Young [4]. Their model differs from the present work on the following points. (1) In the calculation of  $F_{\text{conf}}$ , they make use of the variational perturbation theory with a soft sphere reference potential, as opposed to the WCA theory supplemented by our new potential separations. (2) They treat the internal levels of the molecule in the rigid rotator and harmonic oscillator approximations for the *isolated molecule*, i.e., they do not include density effects on the IPF. (3) Most importantly, we introduce an additional degree of freedom into the model by allowing for

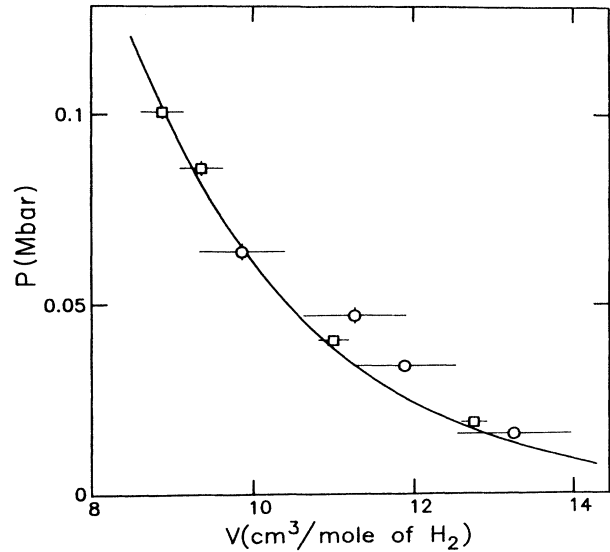


FIG. 4. Single-shock Hugoniot curve of  $\text{H}_2$ . The experimental data is drawn from Refs. [22] (squares) and [23] (circles). The solid curve shows the theoretical Hugoniot curve derived from the model given by Eq. (24). Points along the curve are given in Table III.

molecular dissociation, which we find is *not* negligible in the double-shock Hugoniot curve of deuterium (see Tables III and IV).

## VIII. RESULTS AND DISCUSSION

We have applied the free-energy model [Eq. (24)] in the domain  $-6 < \log_{10}\rho \lesssim 0$  and  $2.10 < \log_{10}T < 4.26$ . Below  $\log_{10}T \approx 3.3$ , hydrogen is purely molecular, and our equation of state reproduces previous calculations [4]. At temperatures above  $\log_{10}T \approx 4.1$ , temperature ionization becomes important, and pressure ionization takes place around  $\log_{10}\rho \approx 0$ . We present a subset of our results in Tables V–VII for three isotherms showing the effects of temperature and pressure dissociation. For each density point in the table, we give the concentration of atomic H at chemical equilibrium, along with the total pressure, internal energy, and entropy.

TABLE III. Points along the hydrogen Hugoniot curve of Fig. 4, computed from our model. The last column gives the concentration of H atoms,  $x_{\text{H}} = N_{\text{H}}/(N_{\text{H}} + N_{\text{H}_2})$ .

$T$ (K)	$V$ ( $\text{cm}^3/\text{mol}$ )	$P$ (GPa)	$x_{\text{H}}$
20.18	28.430	$2.97 \times 10^{-3}$	0
266	14.092	0.966	0
431	12.993	1.56	0
722	11.912	2.54	0
1222	10.857	4.14	0
2014	9.808	6.71	$1.77 \times 10^{-5}$
3246	8.742	10.96	$2.41 \times 10^{-3}$

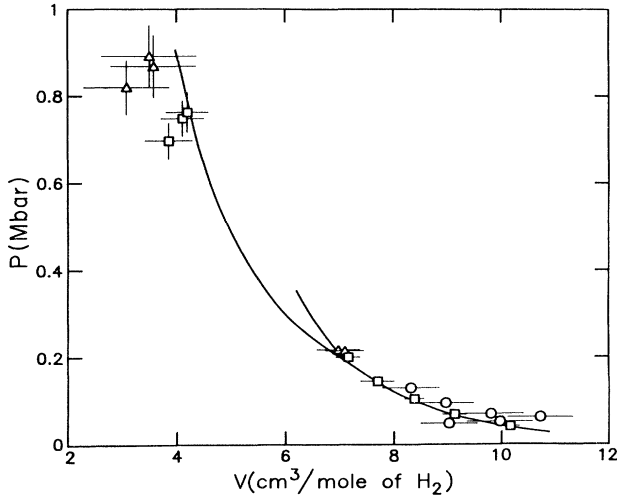


FIG. 5. Single and double-shock Hugoniot curves of  $D_2$ . The experimental data is drawn from Refs. [22] (squares), [23] (circles), and [24] (triangles). The solid curve shows the theoretical Hugoniot curve derived from the model given by Eq. (24) after suitable modifications for deuterium. Points along the curve are given in Table IV.

#### A. Density and temperature dependence of the hard-sphere diameters

Figure 6 shows the density dependence of the hard-sphere diameters for H and  $H_2$  along a few isotherms. The most striking feature in this figure is the strong temperature and density dependence of both  $\sigma_{H_2}$  and  $\sigma_H$ . The two diameters decrease very rapidly with increasing temperature and density, a direct consequence of the softness of the repulsive part of the potential. At low density the diameters depend only on the temperature, whereas at very high density the curves for  $\sigma_H$  reach a value of the order of twice the Bohr radius (and an equivalent di-

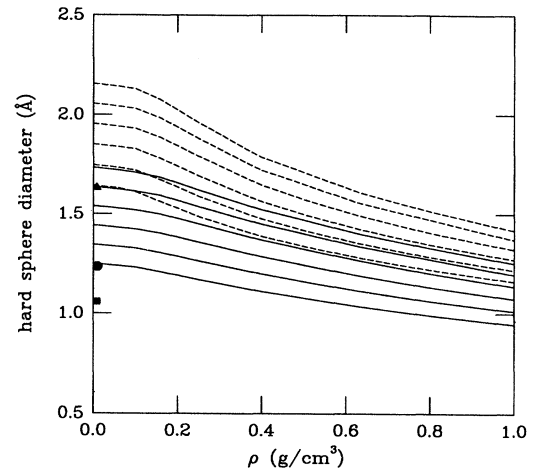


FIG. 6. Hard-sphere diameters of atomic (solid lines) and molecular (dashed lines) hydrogen along isotherms, as derived from the WCA criterion [Eqs. (7a) and (7b)]. In each set of curves, the temperature increases from  $\log_{10}T=3.46$  (top) to  $\log_{10}T=4.26$  (bottom), with a constant spacing of  $\Delta\log_{10}T=0.16$ . The symbols on the left-hand side of the figure indicate the temperature- and density-independent values used in Refs. [57] (square), and [65] (triangle), and [66] (solid circle) for H.

ameter for the molecule), suggesting the imminence of metallization. This indicates that our choice of interaction potentials is reasonable up to these high pressures.

While the hard-sphere diameters are monotonically decreasing functions of density and temperature, their ratio is nearly independent of  $\rho$  and  $T$ :  $\sigma_{H_2}/\sigma_H \approx 1.2-1.3$ , i.e., one molecule occupies about the same volume as two atoms. This arises from the similarity of the repulsive parts of the potentials  $\phi_{H_2-H_2}$  and  $\phi_{H-H}$  [Fig. 2(a)].

In the companion paper, we discuss the phenomenon of pressure *ionization* in depth and compare our results

TABLE IV. Points along the deuterium Hugoniot curves of Fig. 5, computed from our model. The last column gives the concentration of D atoms,  $x_D = N_D / (N_D + N_{D_2})$ .

$T$ (K)	$V$ ( $\text{cm}^3/\text{mol}$ )	$P$ (GPa)	$x_D$
20.23	23.600	$5.65 \times 10^{-4}$	0
555	10.890	2.87	0
978	9.870	4.75	0
1674	8.856	7.83	$1.2 \times 10^{-6}$
2881	7.821	13.3	$8.81 \times 10^{-4}$
4136	7.100	19.3	0.013
4781	6.792	22.6	0.029
6500	6.167	31.8	0.096
7500	5.921	36.9	0.141
Double shock, reflected from 7.10 $\text{cm}^3/\text{mol}$			
4500	5.860	30.5	0.022
5500	4.474	59.8	0.061
6558	3.851	87.8	0.110

TABLE V. Equation of state along the  $\log_{10}T=3.46$  isotherm. For each density  $\rho$ , the entries are the number concentration of atoms, the pressure, the internal energy, and the entropy.

$\log_{10}\rho$ (g/cm <sup>3</sup> )	$x_H$	$\log_{10}P$ (erg/cm <sup>3</sup> )	$\log_{10}U$ (erg/g)	$\log_{10}S$ (erg/g K)
-4.0	$3.0709 \times 10^{-2}$	7.0824	11.5791	8.9864
-3.0	$9.8613 \times 10^{-3}$	8.0800	11.5523	8.9371
-2.0	$3.1183 \times 10^{-3}$	9.1006	11.5455	8.8842
-1.5	$1.7396 \times 10^{-3}$	9.6546	11.5499	8.8538
-1.0	$9.9680 \times 10^{-4}$	10.3311	11.5775	8.8160
-0.6	$9.1813 \times 10^{-4}$	11.0980	11.6933	8.7727
-0.2	$6.1927 \times 10^{-3}$	12.0686	12.0840	8.7129
0.0	$1.0931 \times 10^{-1}$	12.5436	12.3716	8.6939

with other work of similar scope. Since they have all used one form or another of the hard-sphere model to account for interactions between neutral species, we discuss briefly their choice of hard-sphere diameters in light of our results. All these calculations use fixed diameters which do not depend on the density and the temperature (Fig. 6). The value of  $\sigma_H$  used by Ebeling and Richert [65] (triangle) corresponds to the low-density value of one of our coolest isotherms, where the abundance of H atoms is found to be small (see Fig. 7). Then this choice of  $\sigma_H$  seems too large. Since the hard-sphere free energy and pressure behave in first approximation as  $\rho\sigma^3$ , we expect the derived free energy and pressure to be largely overestimated. This can have severe consequences on the thermodynamics of the system, especially on pressure dissociation and ionization. On the other hand, the size of the H atoms appears underestimated in the calculation of Mihalas, Däppen, and Hummer [57] (square), leading to the opposite conclusion. This explains why they had to introduce an *ad hoc* modification of the configuration free energy to induce pressure ionization at low temperatures. Their hard-sphere diameter for the ground state of the molecule, however, is 2.90 Å (not shown on Fig. 6) which is a relatively large value. This combination of large  $\sigma_{H_2}$  and small  $\sigma_H$  favors pressure dissociation and works against pressure ionization. This relatively extreme choice of diameters explains why Mihalas, Däppen, and Hummer find fully pressure-dissociated hydrogen prior to pressure ionization, a major qualitative difference be-

tween their results and the present work. On the other hand, the hard-sphere diameter chosen in Ref. 66 for the H atom (solid circle), applied at  $\log_{10}T \gtrsim 4.1$  is in better agreement with our high-temperature values. In view of our calculations, it appears that these interaction models [57,65] are too crude for a reasonable description of this high-density regime and would probably fail to reproduce the experimental data presented in Sec. VII.

### B. Molecular dissociation

Figure 7 shows the atomic hydrogen concentration  $x_H$  as a function of density for the same isotherms as Fig. 6 (solid lines). Between  $\rho \approx 10^{-4}$  and  $10^{-1}$  g/cm<sup>3</sup>, it shows strong recombination as given by the Saha equation. At higher densities, strong nonideal correlation effects come into play, affecting the internal levels and favoring molecular dissociation and ultimately leading to pressure ionization. Temperature dissociation effects are clearly displayed by the low-density part of the isotherm sequence.

A striking feature of Fig. 7 is that pressure dissociation occurs over a relatively narrow density range which is independent of temperature. This indicates that pressure dissociation is a *pure density effect*, an intuitively predictable result. This probably originates in the similar behavior of the repulsive parts of the H-H and H<sub>2</sub>-H<sub>2</sub> potentials and the nearly constant ratio of the molecular and atomic hard-sphere diameters, as mentioned above. The

TABLE VI. Equation of state along the  $\log_{10}T=3.78$  isotherm. For each density  $\rho$ , the entries are the number concentration of atoms, the pressure, the internal energy, and the entropy.

$\log_{10}\rho$ (g/cm <sup>3</sup> )	$x_H$	$\log_{10}P$ (erg/cm <sup>3</sup> )	$\log_{10}U$ (erg/g)	$\log_{10}S$ (erg/g K)
-4.0	$8.7175 \times 10^{-1}$	7.6442	12.3847	9.1547
-3.0	$5.6867 \times 10^{-1}$	8.5423	12.2199	9.0607
-2.0	$2.5873 \times 10^{-1}$	9.4729	12.0626	8.9755
-1.5	$1.5862 \times 10^{-1}$	9.9883	12.0158	8.9388
-1.0	$9.5754 \times 10^{-2}$	10.6002	12.0013	8.9018
-0.6	$7.5364 \times 10^{-2}$	11.2568	12.0514	8.8683
-0.2	$1.2001 \times 10^{-1}$	12.1103	12.2803	8.8310
0.0	$2.3739 \times 10^{-1}$	12.5561	12.4827	8.8166
0.2	$3.5616 \times 10^{-1}$	13.0054	12.7096	8.7996

TABLE VII. Equation of state along the  $\log_{10}T=4.10$  isotherm. For each density  $\rho$ , the entries are the number concentration of atoms, the pressure, the internal energy, and the entropy.

$\log_{10}\rho$ (g/cm <sup>3</sup> )	$x_H$	$\log_{10}P$ (erg/cm <sup>3</sup> )	$\log_{10}U$ (erg/g)	$\log_{10}S$ (erg/g K)
-4.0	$9.9714 \times 10^{-1}$	8.0154	12.5680	9.1998
-3.0	$9.7325 \times 10^{-1}$	9.0062	12.5567	9.1426
-2.0	$8.2624 \times 10^{-1}$	9.9583	12.4946	9.0693
-1.5	$6.6910 \times 10^{-1}$	10.4274	12.4378	9.0264
-1.0	$4.8759 \times 10^{-1}$	10.9464	12.3879	8.9828
-0.6	$3.6578 \times 10^{-1}$	11.4772	12.3855	8.9480
-0.2	$3.2618 \times 10^{-1}$	12.1878	12.4955	8.9127
0.0	$3.6017 \times 10^{-1}$	12.6020	12.6216	8.8958
0.2	$4.1035 \times 10^{-1}$	13.0344	12.7934	8.8780

influence of the repulsive part of the potentials on our results will be examined in Sec. VIII C.

Molecules are still the dominant species ( $\gtrsim 60\%$ ) at high densities, whereas hydrogen atoms are nearly absent for  $\log_{10}T \lesssim 3.5$ . For the three hottest isotherms,  $x_H \approx 1$  at low densities, indicating the necessity of including ionization in the model.

### C. Influence of the interaction potentials

In this section, we explore the sensitivity of our results to the interaction potentials and to the occupation probability formalism. We have recomputed two isotherms ( $\log_{10}T=3.62$  and  $\log_{10}T=3.94$ ) with different free-energy models. The original free-energy model has been modified by including separately the three following changes.

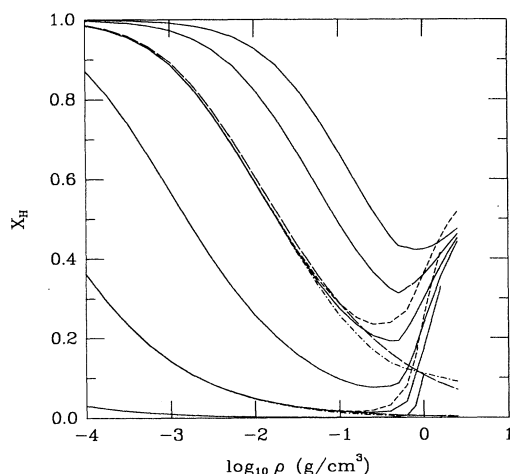


FIG. 7. Concentration of atomic hydrogen along isotherms. The temperature increases from  $\log_{10}T=3.46$  (bottom) to  $\log_{10}T=4.26$  (top), with a constant spacing of  $\Delta\log_{10}T=0.16$ . The solid curves correspond to our free-energy model [Eq. (24)] using the potentials giving by Eqs. (1)–(5) of Ref. [4] and Eq. (2). For the  $\log_{10}T=3.62$  and  $\log_{10}T=3.94$  isotherms, we show the effect of varying the interactions: fluid perturbation theory with softened potentials (short dashes), excluded volume interaction (short dash-dotted), and noninteracting fluid model (long dashes).

(1) For  $\phi_{H_2-H_2}$  we used a new potential derived recently [7] by fitting experimental data up to  $P=0.265$  Mbar. The repulsive part of this potential is reduced by about 10–15% compared with the Young and Ross potential. Also, we roughly account for  $N$ -body effects in the H-H and the H-H<sub>2</sub> potentials by decreasing the stiffness of the *ab initio* potentials arbitrarily by about 20% and 35%, respectively, under the assumption that  $N$ -body effects are more pronounced in nonspherically symmetric systems. The new coefficients are  $s_1=1.5874 \text{ \AA}^{-1}$  and  $\gamma=0.45$  for  $\phi_{H-H}$  and  $s_1=s_2=1.3984 \text{ \AA}^{-1}$ ,  $\gamma=0.55$ , and  $A=10^{-7}$  for  $\phi_{H-H_2}$  (see Eq. (2) and Table I). The new hard-sphere radii derived from these softened potentials are less than 4% smaller than the old ones and the ratio  $\sigma_{H_2}/\sigma_H$  is still nearly independent of  $\rho$  and  $T$ .

(2) We removed the nonlinear contribution in our configuration free energy, keeping only the excluded volume interaction, and solved the Saha equation with the occupation probabilities (18) and (22) in the IPF. This is essentially the model developed by HM [17] except that we use temperature- and density dependent hard-sphere diameters.

(3) Finally we performed a pure Saha calculation, truncating the atomic IPF arbitrarily after 200 levels. In this case, the occupation probabilities of all levels are set to unity. This shows the effect of the occupation probability formalism best.

Figure 7 exhibits the sensitivity of pressure and temperature dissociation on the interaction model. When compared to  $\phi_{H_2-H_2}$ , the new  $\phi_{H-H}$  is not as repulsive as in the original calculation. As a consequence, the softened potentials increase pressure dissociation, but by less than 10%. As expected, the onset of pressure dissociation is shifted to slightly lower densities, but it still occurs over a narrow density range for both isotherms. On the other hand, the two Saha-like models fail completely at high density where they predict complete recombination, a well known shortcoming of this theory. This stresses the necessity of the inclusion of nonlinear effects in the configuration free energy at high density. It also shows that a simple excluded volume interaction cannot lead to pressure ionization. At odds with this result, Mihalas, Hummer, and Däppen [57] have no difficulty in reaching full pressure dissociation. We attri-

bute this apparent discrepancy to their rather large value of  $\sigma_{\text{H}_2}$  (which makes the interaction between molecules much stronger) and to their relatively small value of  $\sigma_{\text{H}}$ , a combination which will strongly favor dissociation.

As expected, the softened potentials lead to lower pressures for given  $\rho$  and  $T$ . The two equations of state depart from each other above  $\log_{10}\rho \approx -0.6$  but the difference remains below 25% even at the highest densities ( $\log_{10}\rho = 0.4$ ).

Figure 8 shows the influence of these various interaction models on the internal energy,  $U$ . At low density all models recover the perfect gas limit. This limit can be seen for the coolest isotherm ( $\log_{10}T = 3.46$ ) where  $U$  is independent of density. Hotter isotherms depart from this behavior because of temperature dissociation, which brings a density dependence to  $U$ . The  $\log_{10}T = 3.94$  isotherm computed with 200 levels in the H atom and occupation probabilities of unity (upper long-dashed line) has a higher internal energy than the other three models. This is caused by increased thermal excitation of the internal levels of H which is not hindered by the effective cutoff of the occupation probabilities. Note that the thermal excitation of H is still fairly low at this temperature (Table IX) and that limiting the partition function of H to the ground-state level with  $\omega_1 = 1$  would bring it into better agreement with the other model, at low density. At high densities, the repulsive forces between particles become dominant and the internal energy rises steeply with density. Again, the calculation based on softened potentials has a slightly lower internal energy, as expected. As discussed above, the model with no interactions (long dashes) tends to full recombination at high densities, where it reaches a constant internal energy value. The model with only excluded volume interaction (dot-

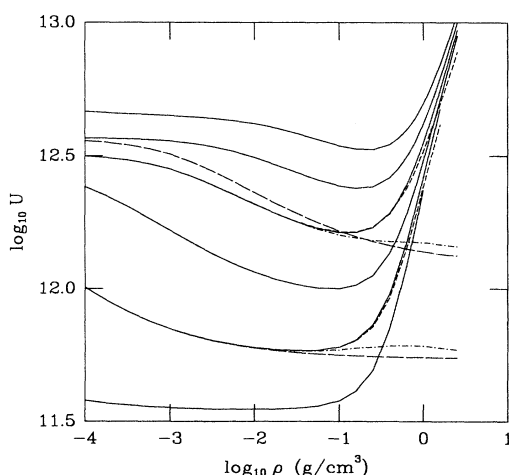


FIG. 8. Internal energy isotherms along the same isotherms as in Fig. 7. The temperature increases from bottom to top. The solid curves correspond to our free-energy model using the potentials given by Eqs. (1)–(5) of Ref. [4] and Eq. (2). For the  $\log_{10}T = 3.62$  and  $\log_{10}T = 3.94$  isotherms, we show the effect of varying the interactions: fluid perturbation theory with softened potentials (short dashes), excluded volume interaction (short dash-dotted), and noninteracting fluid model (long dashes).

dashed), which is linear in density, lies between the two extremes we have just discussed, but it fails completely to reproduce the rapidly rising internal energy obtained with realistic potentials. As we will see below, these nonlinear interactions are essential in the description of pressure dissociation, and ultimately pressure ionization.

#### D. Relative importance of the different contributions to the free energy

Figure 9 shows the relative importance of the different contributions to the free energy along representative isotherms. The vertical scale is the logarithm of the absolute value of the free energy per proton (bound or unbound) in units of  $kT$ . The absolute value is required since the free energy can change sign along an isotherm. Some of the curves are interrupted at the zero crossing point, where the logarithm diverges. Positive and negative contributions to the free energy are labeled ( $>0$ ) and ( $<0$ ), respectively. The various contributions to the total free energy are as follows:  $F$  is the total free energy (thick solid curve);  $F_1$  is the ideal, translational contribution;  $F_2$  is the internal free energy of hydrogen molecules and atoms, including the occupation probability formalism;  $F_3$  is the configuration free energy of the H-H<sub>2</sub> mixture (hard-sphere free energy and perturbation), without the linear, excluded-volume part of the hard-sphere free energy, which is implicitly included in  $F_2$  [see Eq. (15)];  $F_4$  is the quantum correction for atoms and molecules. Note that the behavior of these curves reflects not only the density dependence of the corresponding terms but also the variations in chemical equilibrium along the isotherm as shown in Fig. 7. It is possible to isolate the intrinsic behavior of the free-energy contributions in regimes where the chemical equilibrium is nearly independent of  $\rho$  and  $T$ .

Figure 9(a) shows the  $\log_{10}T = 3.46$  isotherm which is purely molecular for  $\log_{10}\rho \lesssim -0.2$  (see Table I) except for a small amount of atoms at the very low-density end. The molecular fluid is nearly ideal up to  $\log_{10}\rho \approx -1$ , as indicated by the small value of  $F_3$ . The total free energy is essentially the sum of the translational and the internal structure contribution of the molecules. The configuration free energy arising from the fluid perturbation theory is the sum of the hard-sphere reference free energy and of the HTA term, both of which are linear in  $\rho$  in this regime. The linear part of the former is absorbed in the  $F_2$  curve, via the occupation probability. All that remains in  $F_3$  is the linear HTA term, which reflects the attractive part of the potential at these densities. Hence  $F_3$  is negative. As the density is raised, the (positive) nonlinear contribution of the hard-sphere energy increases and ultimately overcomes the attractive contribution. At still higher densities ( $\log_{10}\rho > -1$ ), the potential separation of Kang *et al.* [48] takes precedence and the HTA term itself becomes positive, and grows with density to become even larger than the nonlinear hard-sphere contribution. At this point, the fluid is strongly nonideal, and the total free energy is dominated by  $F_3$ . Because of the strong density dependence of  $F_3$ , it is clear that the pressure arising from the configuration terms is much

larger than the ideal gas pressure near  $\log_{10}\rho \approx 0$ .

The behavior of the HTA term shows that the softness of the repulsive part of the potentials plays a major role at these high temperatures and densities. This fact is also supported by the density and temperature dependence of the hard-sphere diameters (Fig. 6). This observation completely invalidates models based on pure hard-sphere interactions, even corrected with a van der Waals attraction term when modeling the microphysics of fluids at high density or high temperature.

The effect of these strong, nonideal interactions is also felt in  $F_2$ , as states are removed from the molecular IPF: the occupation probabilities,  $\omega_\alpha$ , decrease with increasing density (Table VIII) hereby raising the molecular internal free energy. The curve on Fig. 9 drops because  $F_2 \leq 0$ . With our choice of reference points for the energy of internal states  $\varepsilon_0$ , the vibrational and rotational states of

$\text{H}_2$  mostly lie at  $\varepsilon_\alpha < kT$ , while the opposite is true for the atomic states. As a consequence, the molecular internal free energy is negative and the atomic contribution is positive over the whole range of temperature and density considered here, and as a rule, the  $F_2$  contribution rises with the concentration of atoms. This can be seen in Fig. 9(a) for  $\log_{10}\rho < -3$  where a small amount of atoms is present. At very high densities,  $F_2$  raises rapidly, due to a combination of pressure dissociation and the removal of states from the IPF.

The quantum correction ( $F_4$ ) is always the smallest contribution to the total free energy. At low densities, it increases linearly, but as the hard-sphere diameters start to shrink (Fig. 6), the dependence becomes stronger and its contribution to the pressure is not entirely negligible at low temperatures.

Each of the contributions to the free energy presented

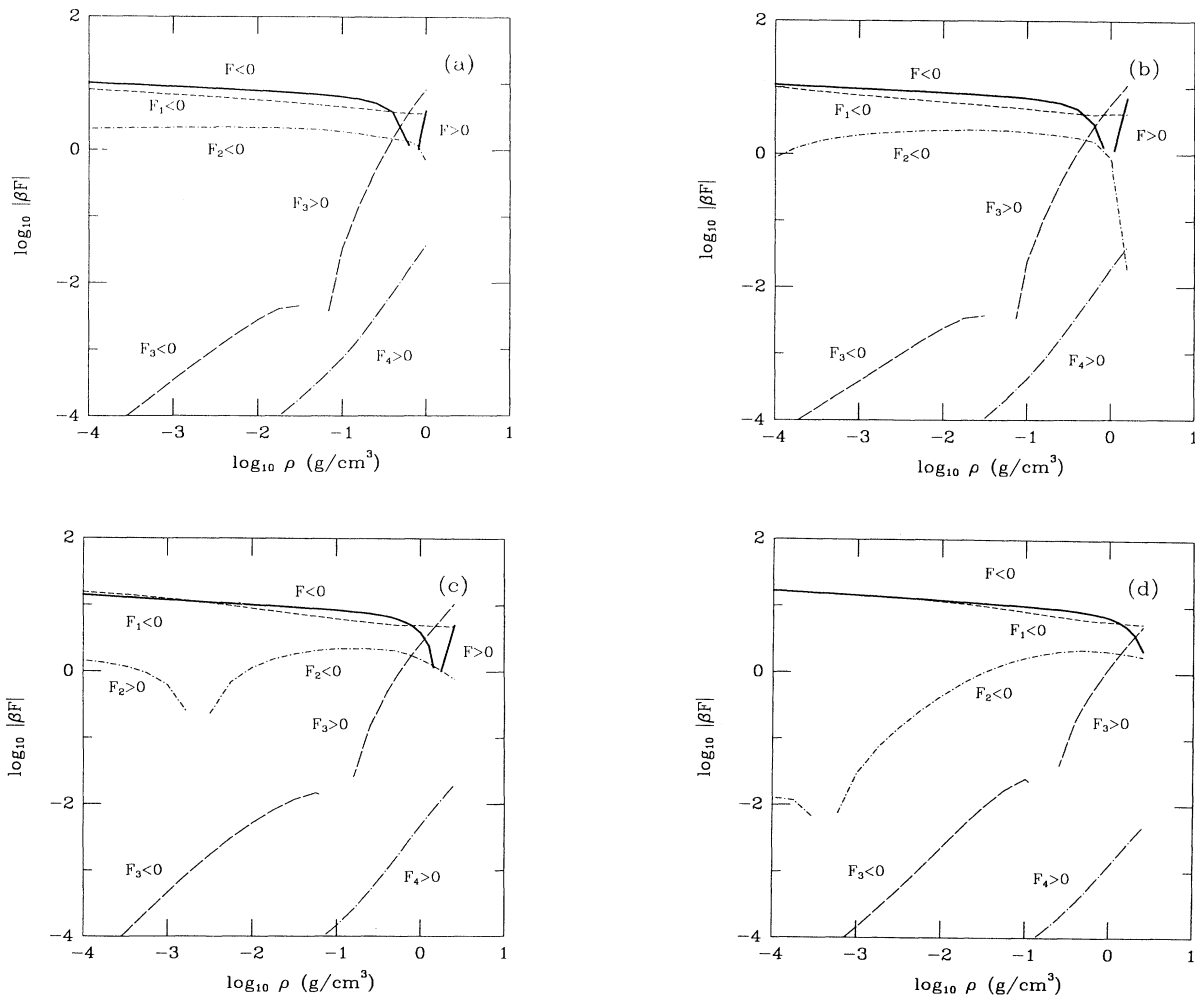


FIG. 9. (a) Individual contributions to the Helmholtz free energy. The quantity plotted is  $\log_{10}|\beta F|$ , where  $F$  is the free energy per proton. The value of  $\log_{10}|\beta F|$  diverges negatively where the free energy changes sign, indicated by a gap in some curves, as for  $F_3$  near  $\log_{10}\rho = -1.3$ . The free energy  $F$  itself is continuous. The total free energy is shown by the thick solid curve. Contributions to the free energy are labeled:  $F_1$ , kinetic (short dashes);  $F_2$ , bound states (short dash-dotted);  $F_3$ , interactions (long dashes); and  $F_4$ , quantum correction (long dash-dotted). This figure corresponds to the  $\log_{10}T = 3.46$  isotherm. (b) Same as (a) for  $\log_{10}T = 3.62$ . (c) Same as (a) for  $\log_{10}T = 3.94$ . (d) Same as (a) for  $\log_{10}T = 4.26$ .

TABLE VIII. Details of the internal partition function of H and H<sub>2</sub> along the log<sub>10</sub>T=3.46 isotherm. The occupation probability of the ground state is ω<sub>1</sub>. A measure of the degree of excitation is given by N<sub>2</sub>/N<sub>1</sub>, the ratio of the populations of the first excited state to that of the ground state. For the molecule, level 2 is the first excited vibrational state.

log <sub>10</sub> ρ (g/cm <sup>3</sup> )	H <sub>2</sub>		H	
	ω <sub>1</sub>	N <sub>2</sub> /N <sub>1</sub>	ω <sub>1</sub>	N <sub>2</sub> /N <sub>1</sub>
-4	0.999	0.134	1.000	5.99 × 10 <sup>-18</sup>
-2	0.940	0.133	0.955	4.08 × 10 <sup>-18</sup>
-1	0.547	0.130	0.642	1.44 × 10 <sup>-19</sup>
-0.6	0.308	0.127	0.407	2.43 × 10 <sup>-21</sup>
-0.2	0.193	0.125	0.259	2.63 × 10 <sup>-23</sup>
0	0.157	0.124	0.212	3.03 × 10 <sup>-24</sup>

in the isotherms shown in Figs. 9(b)–9(d) displays a density dependence which is qualitatively similar to that of Fig. 9(a). The contribution which shows the largest variation is F<sub>2</sub>, a direct consequence of the changes in chemical equilibrium. In addition, as the temperature increases for a given density, the number of excited states increases [see Eq. (12)], leading to larger particles which are more strongly affected by the interactions with their neighbors. By comparing all four figures, we make the following observations.

The temperature dependence of F<sub>3</sub> does not lend itself to a simple analysis in terms of the microphysics. The HTA term has an explicit 1/T dependence and at high density, there is also an implicit temperature dependence in the hard-sphere reference system and in the HTA contribution, via the hard-sphere diameters, σ<sub>ij</sub>, the break point of the H-H<sub>2</sub> potential, λ<sub>12</sub>, and the pair distribution functions g<sub>ij</sub><sup>HS</sup>(r). As expected, F<sub>3</sub> generally decreases as the gas becomes more ideal at higher temperatures. Nevertheless, the configuration free energy still contributes substantially to the total free energy and cannot be neglected.

The temperature dependence of the internal free energy (F<sub>2</sub>) is rather complicated. To appreciate the interplay of thermal excitation of bound states and the density dependence of the IPF sum, we give the occupation probability of the ground state (ω<sub>1</sub>) and the population of the first excited state relative to the ground-state level of both H and H<sub>2</sub> for two isotherms in Tables VIII and IX. As expected, ω<sub>1</sub> decreases monotonically with increasing ρ and decreasing T. In both cases, the interactions get stronger with larger packing fractions and the ground state is affected more drastically. The ground state is barely perturbed for densities below log<sub>10</sub>ρ ≈ -2. This is true of both H and H<sub>2</sub>. The ratio N<sub>2</sub>/N<sub>1</sub> is a measure of the degree of excitation, combining the effects of thermal excitation and “removal” of states via ω<sub>1</sub> and ω<sub>2</sub>. For the H atom, we consider the first excited electronic level, while for the H<sub>2</sub> molecules, the first excited vibrational level is more meaningful. While the degree of excitation of H<sub>2</sub> is nearly independent of ρ, it rises rapidly with temperature because we are considering temperature of the order of the vibrational temperature of the molecule

TABLE IX. Same as Table VIII for log<sub>10</sub>T=3.94.

log <sub>10</sub> ρ (g/cm <sup>3</sup> )	H <sub>2</sub>		H	
	ω <sub>1</sub>	N <sub>2</sub> /N <sub>1</sub>	ω <sub>1</sub>	N <sub>2</sub> /N <sub>1</sub>
-4	0.999	0.538	1.000	5.00 × 10 <sup>-6</sup>
-2	0.955	0.537	0.969	3.73 × 10 <sup>-6</sup>
-1	0.666	0.528	0.753	4.33 × 10 <sup>-7</sup>
-0.6	0.450	0.520	0.558	3.09 × 10 <sup>-8</sup>
-0.2	0.296	0.511	0.391	1.01 × 10 <sup>-9</sup>
0	0.243	0.506	0.331	1.80 × 10 <sup>-10</sup>
0.2	0.208	0.503	0.289	4.19 × 10 <sup>-11</sup>
0.4	0.186	0.500	0.262	1.39 × 10 <sup>-11</sup>

(≈ 6100 K). Because of the large excitation energy of H, the atoms remain essentially all in the ground state. The N<sub>2</sub>/N<sub>1</sub> ratio for H shows a much stronger dependence on ρ than for H<sub>2</sub>, simply because the ratio of excited- to ground-state diameters [Eqs. (17) and (19)] is much larger for H.

In the low and intermediate density range (log<sub>10</sub>ρ ≲ -1), F<sub>2</sub> increases with T (but log<sub>10</sub>|F<sub>2</sub>| decreases since F<sub>2</sub> < 0) as the atomic concentration increases (see Fig. 7). Since thermal excitation of H is negligible in this regime, it reflects essentially the thermal excitation of H<sub>2</sub> and *temperature dissociation*. For the hottest isotherm [Fig. 9(d)], full dissociation is achieved and F<sub>2</sub> begins to drop, due to the onset of thermal excitation of H [Eq. (12)]. In the high-density regime, temperature dissociation is still present but the main physical effect is the increasing number of excited states in both the atomic and molecular IPF. It stresses the necessity of including *pressure ionization* in the model. Both effects increase the internal free energy, but depending on the sign of F<sub>2</sub>, |F<sub>2</sub>| can either increase or decrease. The quantum contribution decreases monotonically with temperature since F<sub>4</sub> behaves as 1/T in first approximation.

We can summarize the behavior of the different contributions to the free energy as follows.

(1) The fluid is nearly ideal up to log<sub>10</sub>ρ ≈ -2. The effect of strong correlations becomes important and even dominant at higher densities.

(2) The correlation term is essentially linear in ρ and is quite small for log<sub>10</sub>ρ ≲ -2. Then it becomes of the order of the internal structure contribution for -0.5 ≲ log<sub>10</sub>ρ ≲ -0.3 and is the dominant term above the latter value. In this model it is at the origin of pressure dissociation since the particles lie in their electronic ground state at the low temperatures considered here. The configuration energy contribution decreases slowly with T.

(3) For densities less than ρ ≈ 0.5 g/cm<sup>3</sup>, the internal structure contribution is the major contribution to the total free energy besides the pure translational term. It increases with density, first when molecular excited states are removed from the IPF, and then when pressure dissociation occurs. It increases also with temperature, reflecting temperature dissociation and suggesting the imminence of temperature ionization. A consistent treatment of the internal and configuration free energies is

essential for a correct description of these physical effects.

(4) Finally the quantum contribution  $F_4$  is the smallest at all densities and temperatures. This term, however, exhibits a very strong density dependence, leading to a non-negligible contribution to the pressure at high densities and low temperatures.

### IX. CONCLUSION

We have developed a free-energy model for a fluid  $H_2$ -H mixture, which is intended to describe the phenomenon of molecular dissociation, caused by both temperature and pressure effects. This is a highly detailed model for the EOS of a dense mixture of hydrogen molecules and atoms. We have used interatomic and intermolecular interactions based on *realistic* potentials. The configuration free energy is calculated within the framework of a fluid perturbation theory, based on a hard-sphere reference system whose *temperature- and density-dependent* diameters are determined by a *thermodynamic criterion*. The validity of this configuration energy has been assessed by comparison with Monte-Carlo calculations based on the same potentials. The influence of the interactions on the internal levels of atoms and molecules is calculated *self-consistently* with an occupation probability formalism. This free-energy model successfully compares with the available shock-wave experimental results, the 300-K static compression isotherm and reproduces the accurate  $H_2$  EOS of Ref. [4] up to the melting curve. Our model produces pressure and temperature dissociation continuously as either the density or the temperature is raised. Pressure dissociation is found to occur swiftly over a narrow density range which is independent of the temperature, while temperature dissociation is a more gradual effect. Modifying the stiffness of the interaction potentials by 15–35 % does not change qualitatively the results. We find that it is essential to include the nonlinear behavior of the configuration energy

and an occupation probability formalism in the internal partition function for a proper treatment of pressure and temperature dissociation. Moreover, under these extreme thermodynamic conditions, it is necessary to include a suitable treatment of the softness of the repulsive part of the interaction potentials if the model is to be compared successfully with experimental results.

This model represents a significant effort to describe accurately the properties of a dense mixture of interacting atoms and molecules in chemical equilibrium. It has immediate applications in the study of the outer layers of giant planets and the analysis of shock compression experiments on hydrogen, where partial dissociation may occur. Applications of this model to experiments on other diatomic molecules are straightforward. In a future companion paper, we will incorporate this model into a more general model which describes pressure and temperature ionization in hydrogen.

### ACKNOWLEDGMENTS

We wish to thank Hugh M. Van Horn for his continuous interest in this work, F. H. Ree for useful discussions, and F. J. Rogers for his comments on the manuscript.

We are most indebted to D. J. Henderson of the IBM Almaden Research Center, who kindly sent us his hard-sphere pair distribution code for binary mixtures. This work was supported in part by the NSF Grants No. AST-87-06711 and No. PHY-88-08146 and by NASA Grant No. NAGW-1476 through the University of Rochester. D.S. gratefully acknowledges financial support from the Natural Sciences and Engineering Research Council of Canada. We are grateful to the Vice Provost for Computing of the University of Rochester for making available to us the substantial computer resources required to complete this project. The Laboratoire de Physique, Ecole Normale Supérieure, is an "Equipe associée au CNRS."

- 
- [1] H. B. Radousky, W. J. Nellis, M. Ross, D. C. Hamilton, and A. C. Mitchell, *Phys. Rev. Lett.* **57**, 2419 (1986).
- [2] W. J. Nellis, N. C. Holmes, A. C. Mitchell, and M. van Thiel, *Phys. Rev. Lett.* **53**, 1661 (1984).
- [3] D. C. Hamilton, W. J. Nellis, A. C. Mitchell, F. H. Ree, and M. van Thiel, *J. Chem. Phys.* **88**, 5042 (1988).
- [4] M. Ross, F. H. Ree, and D. A. Young, *J. Chem. Phys.* **79**, 1487 (1983).
- [5] R. J. Hemley and H. K. Mao, *Phys. Rev. Lett.* **61**, 857 (1988).
- [6] H. K. Mao and R. J. Hemley, *Science* **244**, 1462 (1989).
- [7] R. J. Hemley, H. K. Mao, L. W. Finger, A. P. Jephcoat, R. M. Hazen, and C. S. Zha, *Phys. Rev. B* **42**, 6458 (1990).
- [8] F. X. Schmider, B. Mosser, and E. Fossat, *Astron. Astrophys.* (to be published).
- [9] J. Christensen-Dalsgaard, W. Däppen, and Y. Lebreton, *Nature* **336**, 634 (1988).
- [10] D. E. Winget and G. Fontaine, in *Pulsations in Classical and Cataclysmic Variables*, edited by J. P. Cox and C. J. Hansen (University of Colorado Press, Boulder, 1982), p. 46.
- [11] C. Friedli and N. W. Ashcroft, *Phys. Rev. B* **16**, 662 (1977).
- [12] B. I. Min, H. J. F. Jansen, and A. J. Freeman, *Phys. Rev. B* **33**, 6383 (1986).
- [13] Throughout this paper,  $\log_{10}T$  is the logarithm of the temperature in K, and  $\log_{10}\rho$  is the logarithm of the mass density in  $g/cm^2$ .
- [14] F. J. Rogers, *Phys. Rev. A* **29**, 868 (1984).
- [15] W. D. Kraeft, D. Kremp, W. Ebeling, and G. Röpke, *Quantum Statistics of Charged Particle Systems* (Plenum, New York, 1986).
- [16] H. C. Graboske, D. J. Harwood, Jr., and F. J. Rogers, *Phys. Rev.* **186**, 210 (1969).
- [17] D. G. Hummer and D. Mihalas, *Ap. J.* **331**, 794 (1988).
- [18] G. Fontaine, H. C. Graboske, Jr., and H. M. Van Horn, *Astrophys. J.* **35**, 293 (1977).
- [19] G. Magni and I. Mazzitelli, *Astron. Astrophys.* **72**, 134

- (1979).
- [20] J. Oliva and N. W. Ashcroft, *Phys. Rev. B* **23**, 6399 (1981).
- [21] W. Däppen, Y. Lebreton, and F. Rogers, *Solar Phys.* **128**, 35 (1990).
- [22] W. J. Nellis, A. C. Mitchell, M. van Thiel, G. J. Devine, and R. J. Trainor, *J. Chem. Phys.* **79**, 1480 (1983).
- [23] R. D. Dick and G. I. Kerley, *J. Chem. Phys.* **73**, 5264 (1980).
- [24] M. van Thiel, L. B. Hord, W. H. Gust, A. C. Mitchell, M. D'Addario, K. Boutwell, E. Wilbarger, and B. Barret, *Phys. Earth Planet. Inter.* **9**, 57 (1974).
- [25] J. von Straaten and J. F. Silvera, *Phys. Rev. B* **37**, 1989 (1988).
- [26] R. L. Mills, D. H. Liebenberg, J. C. Bronson, *J. Chem. Phys.* **68**, 2663 (1978); R. L. Mills, D. H. Liebenberg, J. C. Bronson, and L. C. Schmidt, *ibid.* **66**, 3076 (1977); H. Shimizu, E. M. Brody, H. K. Mao, and P. M. Bell, *Phys. Rev. Lett.* **47**, 128 (1981).
- [27] R. D. Eppers, R. Danilowicz, and W. England, *Phys. Rev. A* **12**, 2199 (1975).
- [28] W. England, J. C. Raich, and R. D. Eppers, *J. Low Temp. Phys.* **22**, 213 (1976).
- [29] G. A. Neece, F. J. Rogers, and W. G. Hoover, *J. Comp. Phys.* **7**, 621 (1971).
- [30] D. Ceperley and B. J. Alder, *Science* **231**, 555 (1986).
- [31] R. J. Hemley, H. K. Mao, and J. F. Shu, *Phys. Rev. Lett.* **65**, 2670 (1990).
- [32] N. W. Ashcroft, *Z. Phys. Chem. Neue Folge* **156**, 41 (1989).
- [33] W. Kolos and L. Wolniewicz, *J. Chem. Phys.* **43**, 2429 (1965).
- [34] A. D. J. Haymet, M. R. Kramer, and C. Marshall, *J. Chem. Phys.* **88**, 342 (1988).
- [35] R. N. Porter and M. Karplus, *J. Chem. Phys.* **40**, 1105 (1964).
- [36] M. S. Shaw, J. D. Johnson and B. L. Holian, *Phys. Rev. Lett.* **50**, 1141 (1983); J. L. Lebowitz and J. K. Percus, *J. Chem. Phys.* **79**, 443 (1983).
- [37] The two papers are not exactly consistent in their definitions of energy units: 1 hartree =  $2 \times$  (ionization energy of a H atom with an infinite proton mass), by definition. This is different from twice the ionization energy of the H atom (0.999 456 hartree).
- [38] T. M. Reed and K. E. Gubbins, *Applied Statistical Mechanics; Thermodynamic and Transport Properties of Fluids* (McGraw-Hill, New York, 1973).
- [39] J. P. Hansen and I. R. McDonald, *Theory of Simple Fluids* (Academic, London, 1976).
- [40] H. C. Andersen and D. Chandler, *J. Chem. Phys.* **53**, 547 (1970); J. D. Weeks, D. Chandler, and H. C. Andersen, *ibid.* **54**, 5237 (1971); *ibid.* **55**, 5422 (1971).
- [41] L. L. Lee and D. Levesque, *Mol. Phys.* **26**, 1351 (1973).
- [42] G. A. Mansoori, N. F. Carnahan, K. E. Starling, and T. W. Leland, Jr., *J. Chem. Phys.* **54**, 1523 (1971).
- [43] G. J. Throop and R. J. Bearman, *J. Chem. Phys.* **42**, 2838 (1965).
- [44] E. W. Grundke and D. Henderson, *Mol. Phys.* **24**, 269 (1972).
- [45] S. I. Sandler, *Chem. Phys. Lett.* **33**, 351 (1975).
- [46] P. J. Leonard, D. Henderson, and J. A. Barker, *Mol. Phys.* **21**, 107 (1971).
- [47] L. Verlet and J. J. Weis, *Phys. Rev. A* **5**, 939 (1972).
- [48] G. S. Kang, C. S. Lee, T. Ree, and F. H. Ree, *J. Chem. Phys.* **82**, 414 (1985).
- [49] D. Saumon, G. Chabrier, and J. J. Weis, *J. Chem. Phys.* **90**, 7395 (1989).
- [50] E. Fermi, *Z. F. Physik*, **26**, 54 (1924).
- [51] R. H. Fowler, *Statistical Mechanics* (Cambridge University Press, Cambridge, London, 1936), pp. 259–260.
- [52] W. L. Weise, D. E. Kelleher, and D. R. Paquette, *Phys. Rev. A* **6**, 1132 (1972).
- [53] B. Grabowski, J. Madej, and J. Halenka, *Astrophys. J.* **313**, 750 (1987).
- [54] S. Hashimoto and N. Yamaguchi, *Phys. Lett.* **95A**, 299 (1983).
- [55] W. Däppen, L. Anderson, and D. Mihalas, *Astrophys. J.* **319**, 195 (1987).
- [56] F. J. Rogers, *Phys. Rev. A* **10**, 2441 (1974).
- [57] D. Mihalas, W. Däppen, and D. G. Hummer, *Astrophys. J.* **331**, 815 (1988).
- [58] L. D. Landau and E. M. Lifshitz, *Course of Theoretical Physics. III. Quantum Mechanics: Non-relativistic Theory*, 3rd ed. (Pergamon, Oxford, 1977).
- [59] T. E. Sharp, *At. Data* **2**, 119 (1971).
- [60] K. P. Huber and G. Herzberg, *Molecular Spectra and Molecular Structure. IV. Constants of Diatomic Molecules* (Van Nostrand, Princeton, 1979).
- [61] G. Herzberg, *Molecular Spectra and Molecular Structure. I. Spectra of Diatomic Molecules*, 2nd ed. (Van Nostrand, Princeton, 1950).
- [62] E. Wigner, *Phys. Rev.* **40**, 749 (1932); L. D. Landau and E. M. Lifshitz, *Course of Theoretical Physics. V. Statistical Physics, Part 1*, 3rd ed. (Pergamon, Oxford, 1980).
- [63] W. H. Press, B. P. Flannery, S. A. Teukolsky, and W. T. Vetterling, *Numerical Recipes, The Art of Scientific Computing* (Cambridge University Press, Cambridge, London, 1986).
- [64] L. D. Landau and E. M. Lifshitz, *Course of Theoretical Physics. VI. Fluid Mechanics* (Pergamon, London, 1959).
- [65] W. Ebeling and W. Richert, *Phys. Lett.* **108A**, 80 (1985); *Phys. Status Solidi* **128**, 467 (1985).
- [66] M. Robnik and W. Kundt, *Astron. Astrophys.* **120**, 227 (1983).
- [67] H. M. Van Horn, *Mitt. Astron. Ges.* **67**, 63 (1986).
- [68] G. I. Kerley, *Phys. Earth. Planet. Inter.* **6**, 78 (1972).
- [69] D. Saumon and H. M. Van Horn, in *Strongly Coupled Plasma Physics*, edited by F. J. Roger and H. E. DeWitt (Plenum, New York, 1987), p. 173.